

DESIGN AND CHARACTERIZATION OF OPTICAL
WAVEGUIDES FOR INTEGRATED LASERS

KENNETH HIAL CHURCH

Bachelor of Science Engineering Physics
Oklahoma Christian University of Science and Arts
Oklahoma City, Oklahoma
1988

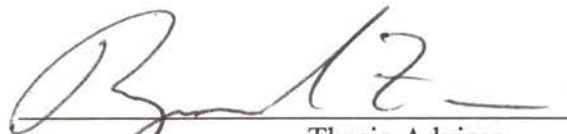
Bachelor of Science Electrical Engineering
Oklahoma Christian University of Science and Arts
Oklahoma City, Oklahoma
1989

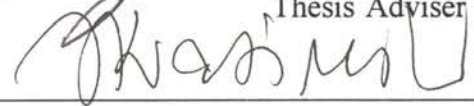
Master of Science Electrical Engineering
Oklahoma State University
Stillwater, Oklahoma
1991

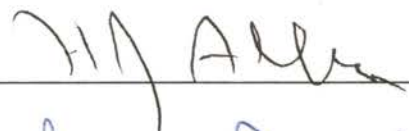
Submitted to the Faculty of the
Graduate College of the
Oklahoma State University
in partial fulfillment of
the requirements for
the Degree of
DOCTOR OF PHILOSOPHY
December, 1994

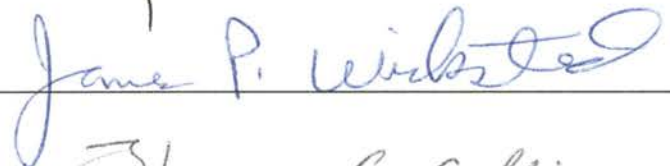
DESIGN AND CHARACTERIZATION OF OPTICAL
WAVEGUIDES FOR INTEGRATED LASERS

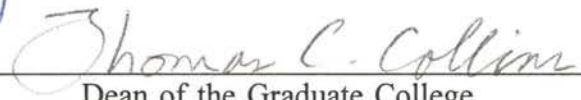
Thesis Approved:



Thesis Adviser








Dean of the Graduate College

PREFACE

This research was conducted to provide new insight into the design of integrated optical devices while fully characterizing those devices. The complete characterization process involves waveguide loss measurements which can now be performed simply and consistently. Direct observation of ion-exchanged waveguides for both planar and channel waveguides can now be done consistently and accurately using X-Ray analysis. A numerical model was used to compare and add insight into the ion-exchange process. The concentration profile obtained from the X-Ray analysis was then used as feedback to control the profile of the waveguide using different fabrication techniques. These characterization techniques were coupled with existing techniques to design an integrated waveguide laser.

I sincerely thank my doctoral committee--Drs. Jack Allison, (Chair), Jerzy Krasinski, James Wicksted and Raymond Zaroni (Dissertation Adviser)--for guidance and support in the completion of this research. I also thank Hial Church for his expert assistance in the laboratory and Michael Moon, Prasad Dasika and Drs. Vladamir Pelekhaty and Rance Fortenberry for their valuable input.

ACKNOWLEDGMENTS

I wish to express my appreciation to Dr Ray Zanoni, my major advisor, for his guidance and expert advice with my research project. He challenged me to learn and understand the project and its significance. My sincere appreciation is extended to Dr Jack Allison for the open encouragement and direction he provided throughout my graduate studies. I would like to thank Dr Jerzy Krasinski and Dr Jim Wickstead for their time and input on this project.

I am especially appreciative to the laboratory technician who is my good friend and father, Hial Church. He provided me with the best technical and personal advice possible during the difficult times. I attribute much of my success to him.

I would also like to express my love and appreciation for my wife, Edie and our three daughters, Cassy, Katie and Kendie for their support and understanding during this challenging time in our life. Thanks also goes to my mom, Bobbie, for her encouragement to finish what I start.

Finally, I would like to thank the Department of Electrical Engineering, the Center for Laser Research and OCAST for their support during my graduate studies.

TABLE OF CONTENTS

Chapter	Page
I. INTRODUCTION	1
Reasons for x-ray microprobe technique	1
Reasons for new optical waveguide loss technique	5
Review of neodymium waveguide lasers	7
II. OPTICAL WAVEGUIDE THEORY	9
Planar Waveguides	9
Channel Waveguides	19
III. WAVEGUIDE PROFILE SHAPING	23
Ion-exchange planar waveguide	25
Burried Waveguides	32
IV. FABRICATION PROCESS	34
Masking Process	34
Polishing	42
V. CHARACTERIZATION OF OPTICAL WAVEGUIDES	50
Electron Microprobe Analysis	51
Optical Profile	69
Modes in Waveguides	69
Waveguide Loss	72
VI. NEODYMIUM WAVEGUIDE LASER	75
Glass Characteristics	75
Ion-exchange	76
Backdiffusion	83

Chapter	Page
Laser Characterization	86
Channel Waveguide Laser	89
VII. SUMMARY, CONCLUSIONS AND RECOMMENDATIONS	95
Summary	95
Conclusions	96
Reccomendations	96
REFERENCES	98
APPENDIX	104
APPENDIX A2.1--FORTRAN CODE FOR SELF CONSISTENCY EQUATIONS	104
APPENDIX A3.1--FINITE DIFFERENCE DERIVATION AND ERROR	107
APPENDIX A3.2--FORTRAN CODE FOR FINITE DIFFERENCE . .	112
APPENDIX A5.1--ANALYTICAL EXPLANATION OF CONVOLUTION	117
APPENDIX A5.2--ANALYTICAL MODEL AND FIT FOR INTERACTION VOLUME	118

LIST OF TABLES

Table	Page
T4.1. Summary of times and procedures for consistent results using photoresist	39
T5.1. Comparison of x-ray results with the manufacturers stated composition	56
T5.2. Summary of x-ray linescan results for Corning 2947	63
T6.1. Summary of fluorescence lifetime measurements	91

LIST OF FIGURES

Figure	Page
2.1. Sketch of a planar waveguide	10
2.2. Sketch of zig-zag pattern made by ray	11
2.3. Modes in a planar waveguide	15
2.4. Index profiles for optical waveguide	16
2.5. Sketch of WKB pattern	18
2.6. Sketch of a channel waveguide	20
2.7. Sketch of two profiles for channel waveguides	22
3.1. Glass melt interface for ion-exchange	24
3.2. Theoretical diffusion profile for constant t	30
3.3. Theoretical diffusion profile for constant m	31
4.1. Photograph of photoresist ridges	38
4.2. Sketch of aluminum lift of process	41
4.3. Sketch of mask for patterning	43
4.4. Overview of fabrication process	44
4.5. Sketch of coupling techniques	46
4.6. Photograph of edges of polished glass	47
4.7. Demonstration of guided light	49

5.1. Model of an atom	53
5.2. EDS spectrum	55
5.3. Sketch of interaction volume	58
5.4. Plot of erfc convolved with gaussian	60
5.5. Fit to determine interaction volume	62
5.6. Plot of Time vs. Diffusion Coefficient	65
5.7. Fit of experimental data	66
5.7. Two dimensional x-ray plot	67
5.9. Two dimensional x-ray plot with dip	68
5.10. Intensity profile of channel waveguide	70
5.11. Mode observation setup	71
5.12. Loss setup and results	73
6.1. APG-1 glass photograph	77
6.2. APG-1 x-ray linescan plot	78
6.3. LG-680 x-ray linescan and photo	80
6.4. BK-7 linescan and fit	82
6.5. S-3 linescan and fit	84
6.6. Backdiffusion photographs	85
6.7. S-3 depletion shown by x-ray	87
6.8. S-3 transmission spectrum	88
6.9. Fluorescence spectrum for S-3	89
6.10. Fluorescence lifetime for S-3	90

6.11. S-3 laser power output 94

CHAPTER I

INTRODUCTION

Just as electronics has made the transition from large vacuum tubes to semiconductors, bulk optical devices are starting to evolve towards integrated optical devices. These integrated optical devices have the advantage of small size, structural stability and polarization stability when compared to gas lasers, solid state lasers or optical beam splitters. Integrated optical devices such as couplers¹⁻⁵, integrated mode locked lasers⁶ or integrated optical switches⁷ begin with a channel waveguide which is fabricated in glass, crystal or semiconductor materials. A channel waveguide guides light by containing the light by total internal reflection. Routing input and output signals, multiplexing and demultiplexing will all be done on a single optoelectronic chip.⁸ Optical processing of the signals received from fibers can be done more cost effectively once the initial design and fabrication of the electro-optic device is completed. The device is then fabricated in a fashion similar to that involving the mass production of semi-conductor devices. A mask and standard process can be made to reproduce the device easily and cheaply.

This paper discusses improvements made in the characterization of optical waveguides. The first is an improvement in the direct observation of the concentration profile by electron microprobe of both planar and channel waveguides. The second is in the loss measurement techniques available. A new technique to measure loss simply,

consistently and accurately is demonstrated. These improved techniques were combined with existing techniques to characterize optical waveguides fabricated in neodymium-doped glass. This provided the necessary information to design an integrated neodymium waveguide laser.

Glass integrated optics is one area which continues to develop product improvements with strong efforts being made to commercialize integrated glass devices. Corning Glass Works Inc, as well as others, is manufacturing fiber splitters for communications using integrated channel waveguides.⁹ National Institute of Standard Technology (NIST) in conjunction with Schott Glass Technologies has patented an integrated Neodymium waveguide laser.¹⁰ Even though much work has been done, areas including characterization and fabrication techniques as well as the development of new glasses need additional improvement.

Ion exchange is a common technique used to strengthen glass. In 1972 a group used this technique for the first time to make a glass waveguide.¹¹ Ion-exchange is a straightforward method to reproduce low loss waveguides in glass. Glass has good optical qualities, is rigid and can withstand large thermal changes. Not all glasses are ion exchangeable, and this must be one of the first considerations when attempting to make glass waveguides. Certain guidelines can be followed when determining which glasses accept ion-exchange and which do not. The host glass composition varies depending on the specific application. A few elements including potassium, sodium, cesium and lithium

are used to add certain desired effects such as changing the softening point or greater resistance to bubble formation. These elements are also not as strongly attached to the molecular structure. Glass containing these elements is optimally ion-exchangeable. Additionally, for two elements to ion-exchange they must contain the same valence and chemical properties.

Glasses which are ion-exchangeable may not guide light because the refractive index may not increase. Those glasses which are capable of guiding light by ion-exchange can be characterized using optical techniques such as the inverse WKB (named after Wentzel, Kramers and Brillouin) method or the effective index method.¹²⁻²⁰ These methods will provide good estimates if the index profile changes are small compared to the wavelength. This information will provide a limited view of the refractive index profile. Direct observation of the profile is the better approach.

Measuring the concentration profile directly will provide information concerning the guided wave mode profile and the number of modes supported by the guide. This in turn is useful for maximizing the coupling efficiency and designing single mode waveguides. The only visible evidence of ion-exchange in a glass is the swelling effect which takes place because its density has increased after the diffusion of ions into the glass matrix. Consequently, we must investigate ion-exchange with X-ray microprobe analysis for accuracy.

Several groups have used some kind of elemental analysis to observe the concentration profile.²¹⁻²⁶ Ramaswamy used a Scanning Electron Microscope (SEM) with a back scatter detector to obtain a scanned profile of silver diffused into different silicate host glasses.²¹⁻²³ This method effectively obtained a qualitative estimate of the profile of the waveguide. Backscatter provides a method for direct observation of both planar and channel waveguide profiles. Numerical modeling and comparisons were made in order to study the refractive index change after ion-exchange. Ramaswamy's group was able to use only silver ion-exchange for analysis because silver is a heavy element and easy to see with a backscatter detector. Lighter elements such as potassium are more difficult to directly observe with a backscatter detector.

The fabrication and characterization of Ag - Na ion-exchanged waveguides has been thoroughly studied by Ramaswamy and other scientists.^{12-14,21-24} A look at K - Na ion-exchange is sequentially the next level of investigation. Since this cannot be effectively done with a backscatter detector, microprobe analysis was used.^{25,26} Ramaswamy and a host of other scientists used this method to observe both Ag and K ions in glass waveguides.^{24,26} Although several different groups have worked with this method, none correctly considered the interaction volume. Only two of groups mentioned it.^{24,26} A group from the U.S. Naval Research Laboratory misstated completely the spatial resolution of their experiment. They claimed the spatial resolution of their microprobe equipment was 700 angstroms (the diameter of the electron beam). They did correct for the profile using this number.²⁴

All of the analysis done with the microprobe were with planar waveguides. The width of the planar waveguides examined directly by either backscatter or x-ray has been as small as six microns when observing Ag - Na ion-exchanged guides.^{23,24} K - Na ion-exchange waveguides are much more difficult to observe. Waveguide widths of twenty to forty microns were used.^{25,26} To date, no direct observation of K - Na six micron planar waveguides has been observed. This paper discusses the characterization of planar waveguides as small as six microns using electron microprobe analysis. The interaction volume will be considered by comparing the experimental results with a numerical model. Observation of a channel waveguide using this technique will also be shown.

Waveguide loss is an important measurement when determining the quality of the waveguide. Several techniques currently exist for measuring waveguide loss.²⁷⁻³⁰ Each technique has its advantages and disadvantages. The cut back method is the standard technique for measuring loss in fiber optic cable.³¹ This method is extremely accurate for fibers since long lengths can be used to begin with. Channel waveguides in substrates are normally one to three centimeters long so there is not much to cut back. This technique is used and does show a certain amount of consistency.²⁷ The major draw back of this method is the obvious destruction which the channel waveguide will undergo. This is also a time consuming measurement since the waveguide must be ground and polished to cut it back.

Another method of loss measurement is the back coupled technique.²⁸ This

method relies heavily on perfect ends which will produce an intensity profile which can be coupled back into the waveguide exactly by use of a mirror. This method was compared against the cut back method and produced consistent results. This is a non-destructive method. Harun et al. claim an accuracy of ± 0.05 dB/cm.

Another technique used is the photothermal deflection technique.²⁹ This method requires a probe laser that hits the channel waveguide orthogonally. The channel will have a source coupled into the waveguide which creates a slight change in the refractive index according to the intensity of the coupled source. This change in the refractive index can be seen by detectors monitoring the probe. This has the advantage of eliminating the coupling factor and looking directly at the guided section. Hickernell et al stated that an accuracy of ± 0.03 dB/cm can be achieved with this method, however the authors of this paper have admitted this technique is complicated to use.

A camera with a frame grabber can be used to capture coupled light in a waveguide.³⁰ A program can then be written to observe waveguide loss by looking at the intensities of each pixel. This method works well for high loss waveguides, but lower loss guides do not produce consistent results. This method is non-destructive and is easy to use.

There are other loss measurement techniques as well, but they are complicated and some have trouble with low loss guides.^{32,33} My waveguide loss technique, once set up,

is easy to use, non-destructive and will observe low loss in guides. This technique uses a microscope objective to gather light at a specific location on the waveguide. The light is focused onto a detector and will scan the waveguide at a discrete number of points. This has the advantages of an adjustable spot size, a maximum intensity near the waveguide, but not on the waveguide which can be found by focusing the lens and an adjustable sensitivity with the aid of a lock-in amplifier.

These characterization techniques can be coupled with transmission spectrum, fluorescence spectrum and fluorescence lifetime to begin the characterization process of an integrated waveguide laser. To fabricate an integrated waveguide laser using ion-exchange a host material must first be chosen which will raise the refractive index after ion-exchange. A study of four different host glasses was done and the results are presented in this paper. Two of these host materials did raise the refractive index in the substrate producing waveguides. A waveguide laser was made from one of these and the results of which are presented in this paper.

Neodymium waveguide lasers have been fabricated by several different groups.³⁴⁻³⁷ A group from NIST fabricated a waveguide laser in a silicate base glass.³⁴ The fabrication process was done with field assist and a mixture of KNO_3 and CaNO_3 to reduce the melting point since a teflon crucible was used to hold the salt bath. Another group from Japan used a glass from HOYA using the silver diffusion technique to fabricate the waveguides.³⁵ A diode laser was used to pump the waveguide laser. A third

group working with neodymium waveguide lasers used potassium ion-exchange to obtain their waveguides and pumped with a Ti:Sapphire laser.³⁶ All of the mentioned waveguides had varying lengths and slope efficiencies. The slope efficiency for the laser must be determined by considering the coupling efficiency of the pump power.

The characterization techniques mentioned above have been applied to the fabrication and design of a working Neodymium waveguide laser. This paper will demonstrate the fabrication and characterization of the waveguides as well as lasing output of the resulting integrated laser.

CHAPTER II

OPTICAL WAVEGUIDE THEORY

Optical waveguides confine light in both one and two dimensions. The theory of optical waveguides will be discussed using the ray optics approach. This will provide the basic understanding of guided wave optics. Numerical modeling of both homogeneous and in-homogeneous waveguides will be explained.

Planar Waveguides

Optical waveguides confine and guide light by total internal reflection. Typical optical waveguides consist of a region of refractive index larger than the surrounding medium. A planar waveguide is demonstrated in Figure 2.1 where there is a region with thickness h and refractive index n_b , surrounded by a refractive indices n_s and n_a . Planar waveguides confine the light in one dimension.

A ray with parallel wavefronts will be confined between two boundaries.³⁸ The ray will be reflected from each interface. This will appear as a zig-zag motion and is demonstrated in Figure 2.2. The ray undergoes total internal reflection if the angle θ shown in Figure 2.2, exceeds the critical angle as given by E2.1.

$$\theta_c = \sin^{-1} \frac{n_2}{n_1} \qquad \mathbf{E2.1}$$

The ray will also undergo a phase shift for each reflection. The phase shifts can

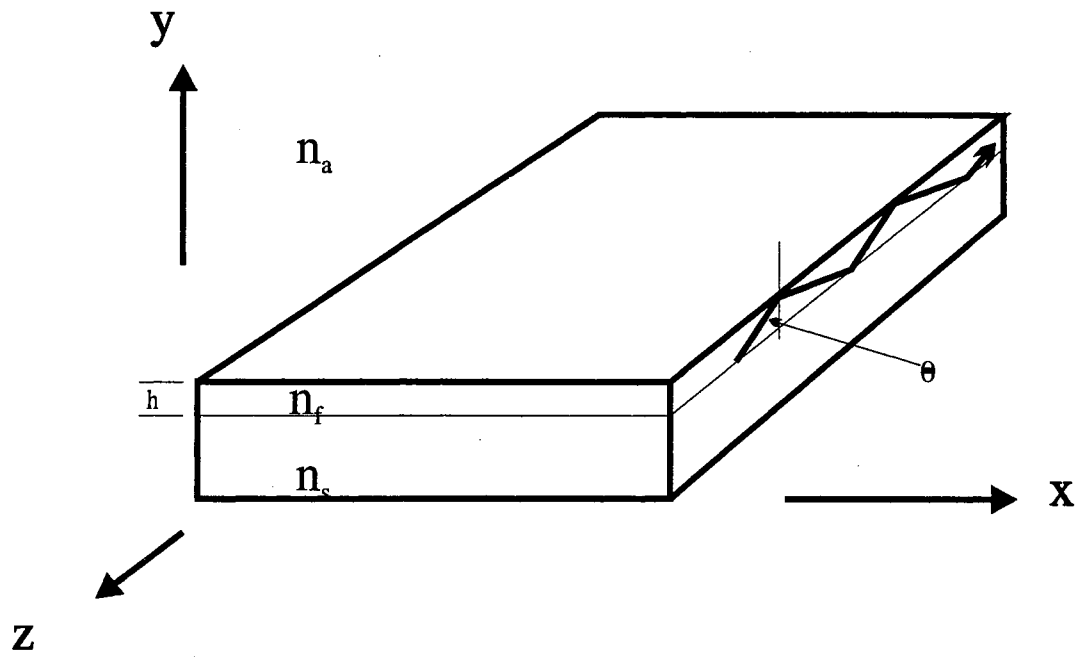


Figure 2.1. Planar waveguide with refractive index n_f . Ray makes a zig-zag pattern with an angle θ .

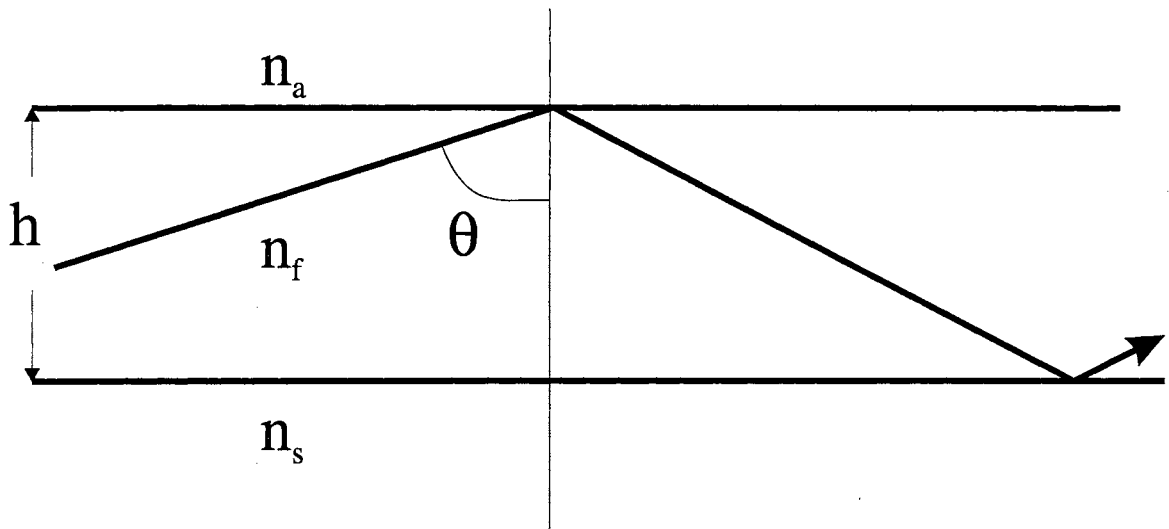


Figure 2.2. Zig-zag pattern made by ray. θ is the angle which the ray will make with the normal to the waveguide.

be obtained from Fresnel's equations. Fresnel's equations, which can be derived from waves at an interface, are written for both polarizations of light in equations E2.2 and

$$R_{TE} = \frac{n_1 \cos \theta - \sqrt{n_2^2 - n_1^2 \sin^2 \theta}}{n_1 \cos \theta + \sqrt{n_2^2 - n_1^2 \sin^2 \theta}} \quad \text{E2.2}$$

E2.3.

$$R_{TM} = \frac{n_2^2 \cos \theta - n_1 \sqrt{n_2^2 - n_1^2 \sin^2 \theta}}{n_2^2 \cos \theta + n_1 \sqrt{n_2^2 - n_1^2 \sin^2 \theta}} \quad \text{E2.3}$$

These equations have only one dependent angle, θ . From this it can be seen that rays incident on a boundary at an angle which exceeds the critical angle will have a complex part. The reflection coefficient can now be written as equation E2.4.

$$r = |r| e^{2j\phi} \quad \text{E2.4}$$

where ϕ is the phase and $|r|$ is the reflected amplitude. The phase shifts for both TE and TM polarizations can be computed from equations E2.2 and E2.3 and written as E2.5 and E2.6. These equations are used to solve for the guided modes.

$$\tan\phi_{TE} = \frac{\sqrt{n_1^2 \sin^2\theta_1 - n_2^2}}{n_1 \cos\theta_1} \quad \text{E2.5}$$

$$\tan\phi_{TM} = \frac{n_1^2}{n_2^2} \frac{\sqrt{n_1^2 \sin^2\theta_1 - n_2^2}}{n_1 \cos\theta_1} \quad \text{E2.6}$$

Plane waves are traveling in the direction of the ray which is perpendicular to the wavefront in an isotropic medium. These plane waves will have a propagation constant given by E2.7, where $k n_f$ is the wave vector for the thin film. The direction of propagation will be in the z-direction as given by Figure 2.1.

$$\beta = k n_f \sin\theta = \frac{\omega}{v_p} \quad \text{E2.7}$$

It should be noted that not all values of θ will satisfy the self-consistency condition. The total phase shift for a round trip, in the y direction, must be an integer multiple of 2π . Taking into consideration the optical path which the ray traverses from the film-substrate interface to the film-air interface and back again and both reflections, equation E2.8 can be written. The phase shift, $k n_f \cos\theta$, is for the wave traveling from the film-substrate interface to the film-air interface. The phase shift, $-2\phi_a$, is incurred during the reflection from the film-air interface. A second phase shift, $k n_f \cos\theta$, will occur for the passage back to the film-substrate interface. The last phase shift to consider is from the reflection off of the film-substrate interface, which is given by $-2\phi_s$. This completes the round trip and satisfies self-consistency.

$$2kn_f h \cos\theta - 2\phi_s - 2\phi_c = 2v\pi \quad \text{E2.8}$$

Coupling equation E2.8 with equations E2.5 or E2.6, the number of modes can be determined numerically. The number of modes which a waveguide will support depends the refractive indices of the film, substrate and cover, the film thickness and the wavelength of the incident light. These equations were solved numerically to determine the effective index of each mode. The effective index for a mode is given by E2.9.

$$n_{eff} = n_f \sin\theta \quad \text{E2.9}$$

A plot can be made to indicate the number of modes over a range of thicknesses and effective indices. This plot is shown in Figure 2.3 and the fortran program which provided the numerical results is listed in the appendix, A2.1. The plot given in Figure 2.3 is for a step index profile. A step index profile can be made using spin coating or RF sputtering. Ion-exchanged waveguides has a graded index profile. Two different processes will be considered for profiling. The first is the thermal ion-exchange which produces an index profile represented by the complementary error function (erfc). The second method of ion-exchange is to apply both heat and an electric field, this is known as field assist ion-exchange. Field assist can be done by applying a voltage across the substrate while heating. This technique will push the ions deeper into the glass producing a flat top with a complementary error function tail. The three profiles are shown in Figure 2.4 for comparison. The thermal and field assist ion-exchange will produce a non-uniform refractive index or an inhomogeneous medium. The refractive index can be

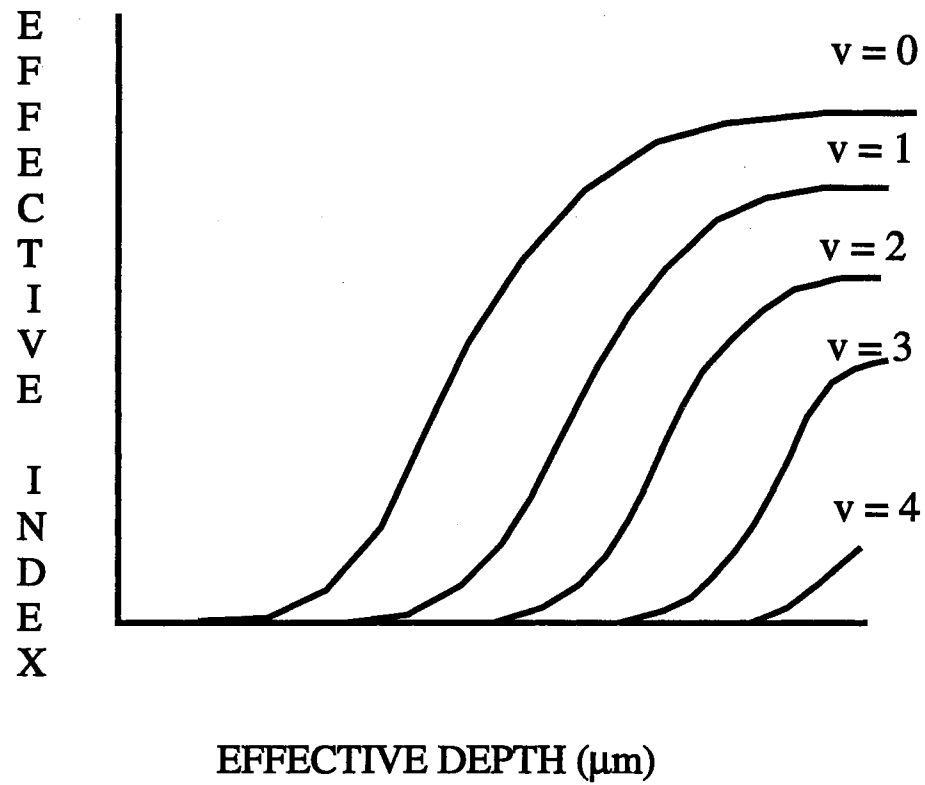


Figure 2.3. Plot of Effective Depth vs Effective Index. A discrete number of modes are obtained from a planar waveguide.

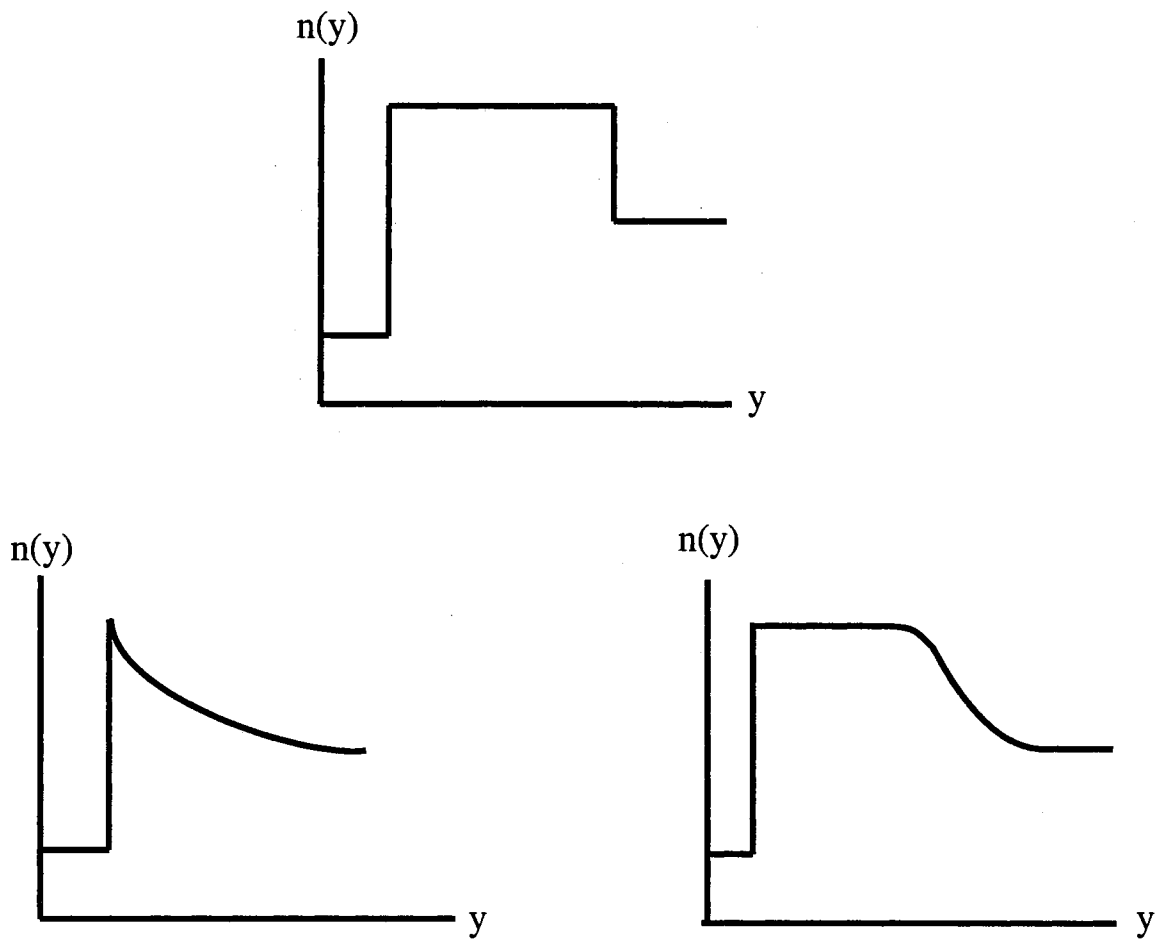


Figure 2.4. Refractive index profiles. Step index, erfc index and extended erfc. The second two are obtained from the ion-exchange process.

described, in the case of the planar waveguide, as $n = n(y)$.

The inhomogeneous waveguide boundaries have an effective thickness which can normally be estimated at $1/e$ from the peak of the refractive index profile. It is the profile of the refractive index which will determine the mode profile. The refractive index profile must be considered when designing waveguides to mode match fiber optic cable.

Obtaining a solution for the effective index of a graded index waveguide is done using the WKB method. The WKB method was originally used to solve Schrodinger's equation.³⁹ This method is only valid if the change in refractive index is small compared to the wavelength. The same methodology as the step index solution is used, except the optical path is not a straight line and the turning points must be redefined. Figure 2.5 displays the exponential profile and the optical path which the ray follows.

At points A and B the phase shift will be the same as described by the step index profile. At point C there is no discontinuity, therefore the phase shift is given by $\pi/2$. The optical path with phase shifts can be determined by E2.10.

$$\int_A^B \kappa(x) dx - 2\phi_1 - 2\phi_2 = 2m\pi \quad \text{E2.10}$$

Using symmetry and integrating from point A to C the equation to determine the effective index is given in E2.11.

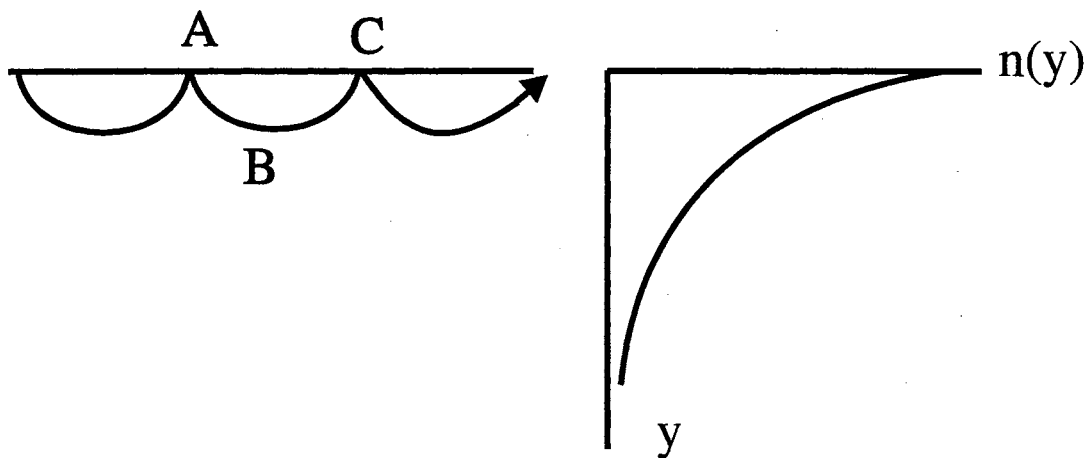


Figure 2.5. WKB method to solve the consistency equation for an inhomogeneous waveguide. The plot on the right is the refractive index profile. The picture on the left is the optical path which the ray will follow.

$$2 \int_A^C [k_o^2 n^2(x) - \beta^2]^{1/2} dx - \frac{\pi}{2} - 2 \tan^{-1} \sqrt{\frac{\beta^2 - k_o^2 n_c^2}{k_o^2 n_f^2 - \beta^2}} = 2m\pi \quad \text{E2.11}$$

This can be solved numerically obtaining several solutions for differing effective thicknesses. This method is useful for determining a specified propagation constant β_v . This will require a known index profile $n(y)$. If several propagation constants are known then this method can be applied in reverse to determine the profile shape.

Channel waveguides

Confining the light in two dimensions will produce a channel waveguide. The most common and commercially used channel waveguide is the fiber optic cable. This waveguide is flexible and can be used to guide light over long distances or can be coiled around objects. A fiber optic waveguide has a circular profile which can be solved analytically and additionally fiber optic cable is good for carrying signals over long distances. Fiber optic cable is neither rigid nor easy to splice together to make electro-optic devices. Using a fiber optic cable to connect the electro-optic devices is required, therefore matching the mode profiles is important.

A channel waveguide in a glass substrate is shown in Figure 2.6. The larger the channel the more guided modes the channel will support. The total number of modes a channel waveguide will support is determined by the height and the width of the channel.

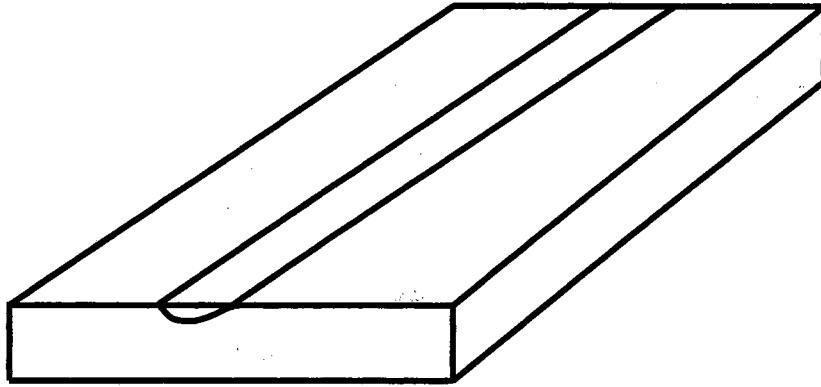


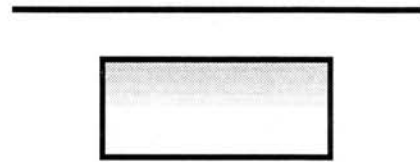
Figure 2.6. Ion-exchanged channel waveguide in a glass substrate. The channel waveguide will confine light in two dimensions.

Making rigid, non-flexible channel waveguides can be accomplished with several different techniques. The channel waveguides discussed in this paper are the result of ion-migration in glass. These waveguides will be confined in the x and y directions. Figure 2.7 displays the embedded and buried waveguides. The embedded waveguide can be made using thermal and field assist ion exchange. The buried guide can be made by back diffusing ions into the substrate after the first ion-exchange or by removing the substrate after the initial ion-exchange and applying heat and an electric field.

Figure 2.7 displays schematic profiles for channel waveguides. As stated earlier the profile for the ion-exchanged waveguide is a graded index. A rounding effect will occur as the ions migrate into the glass substrate. This rounding effect is desirable since fiber optic cables are circular. A fiber optic cable is the major source of input and output coupling for the integrated optical devices being made .



Embedded



Buried

Figure 2.7. Ion-exchanged waveguides using thermal ion-exchange, field assist ion-exchange and backdiffusion.

CHAPTER III

WAVEGUIDE PROFILE SHAPING

The refractive index profile of the waveguide depends upon the method used to raise the refractive index. Techniques involving thermal ion-exchange, electric field and ion-milling can be done separately or coupled with each other to control the shape of the profile.⁴⁰⁻⁴³ The substrate is made of a multi-component oxide glass.⁴⁴ This is known as the host material and will be comprised of a network former such as SiO_2 , B_2O_3 , GeO_2 , P_2O_5 or AsO_3 . The network former is the strong bond between the cation and the oxygen atom. Other composite atoms such as ZnO and PbO are known as intermediate formers and can be added for strength. The last piece of the glass composition will be the weakly bonded network modifiers. It is these network modifiers, Na_2O , CaO , K_2O and Li_2O , which will ion-exchange when placed in the salt bath. When the temperature is raised the ion mobilities of the network modifiers increase. This coupled with a salt bath containing ions which are of the same valence and chemical properties promotes random collisions at the interface. At the glass-melt interface both of the ion concentrations initially drop to zero. A picture representing the glass-melt interface is shown in Figure 3.1. The non-equilibrium situation starts the ion-exchange process. The two similar cations will work toward an equilibrium stage. Ions moving out of the glass move freely and rapidly away from the substrate. Ions from the salt bath diffuse into the substrate. If the salt bath is removed but the temperature is kept high, the migration of the alien ion continues to work its way into the glass. Once the heat is removed the ions become much

SALT BATH

GLASS

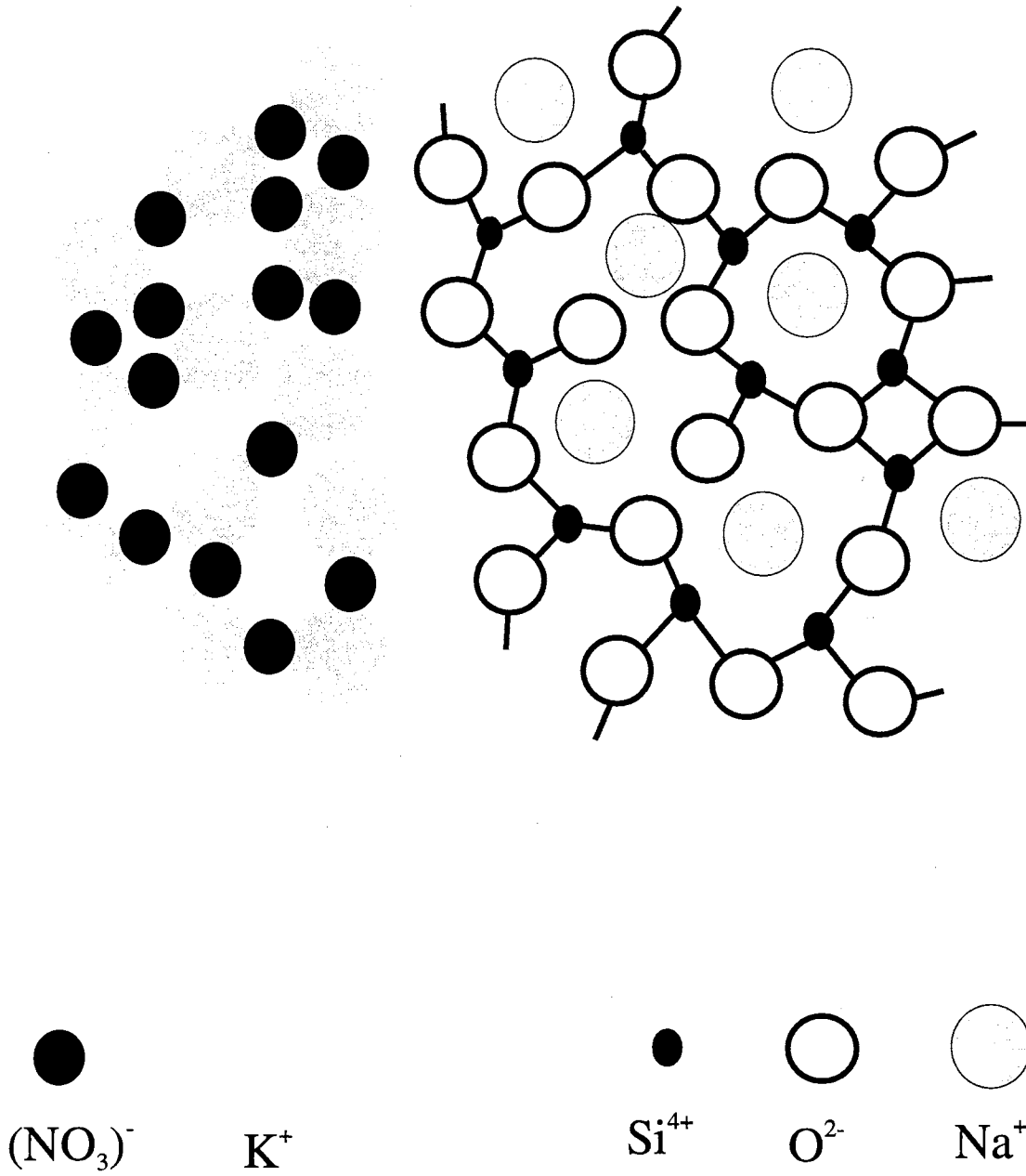


Figure 3.1. Diagram of glass-melt interface.

less mobile and the ion concentration becomes frozen into the glass.

When an electric field is applied in addition to heat, the ion-exchange takes place in a more controlled way. The electric field will define the direction of ion-diffusion. The similar cations are the charge carriers, causing both of the cations travel in the same direction. The salt bath cation will go into the glass substrate and the glass ion will exit through the cathode end. The higher the temperature and voltage, the faster the exchange. The combination of these two can provide some control over the index profile. The profile can be described theoretically using a partial differential equation.⁴⁰⁻⁴⁴ The partial differential equation derives from the physics of the binary exchange inside the glass.

Ion-exchange planar waveguide

An analytic solution for contributions of both thermal ion exchange and electric field can be obtained using the diffusion equations. It should be noted that the electric field can be set to zero and the equation will still be valid producing only the effects of the thermal process. Variables to consider:

D = diffusion coefficient

c = ionic concentration

j = flux of ions

M = ratio of diffusion constants

T = temperature

E = electric field

k = Boltzman's constant

e = charge of proton

f = correlation factor

For this diffusion process it is assumed that a binary ion exchange process exists and the ions are considered to be monovalent. This implies that when one ion leaves the solid glass structure it is replaced by its counter part ion contained in the salt bath, occupying the same space or very nearly the same. Denote the ions to be exchanged by A and B with A usually representing the dopant ion being exchanged into the glass and B is the original ion in the glass. The flux equations can be written as follows:

$$j_A = -D_A \nabla c_A + c_A D_A \frac{eE}{fkT} \quad \text{E3.1}$$

$$j_B = -D_B \nabla c_B + c_B D_B \frac{E}{fkT} \quad \text{E3.2}$$

$$c_A + c_B = c_o \quad \text{E3.3}$$

The condition for the electrical neutrality of the glass is where c_o is the constant total concentration of mobile ions in the glass.

$$\nabla(c_A + c_b) = 0 \quad \text{E3.4}$$

The total ionic flux j_o corresponding to the electrical current density $i = ej_o$ is as follows:

$$j_o = j_A + j_B \quad \text{E3.5}$$

Take equations E3.1 and E3.2 and replace the j_A and j_B in equation E3.5 to obtain the following:

$$j_o = -D_A \nabla c_A + c_A D_A \frac{eE}{fkT} - D_B \nabla c_B + c_B D_B \frac{eE}{fkT} \quad \text{E3.6}$$

let $p = eE/fkT$ and then solve for p giving:

$$p = \frac{j_o + D_A \nabla c_A + D_B \nabla c_B}{c_A D_A + c_B D_B} \quad \text{E3.7}$$

using a self-diffusion constant given by $M = D_A/D_B$ and multiplying equation E3.7 by D_B/D_B produces the following:

$$p = \frac{\frac{j_o}{D_B} + \frac{D_A}{D_B} \nabla c_A + \nabla c_B}{\frac{D_A}{D_B} c_A + c_B} \quad \text{E3.8}$$

$$p = \frac{\frac{j_o}{D_B} + M \nabla c_A + \nabla c_B}{M c_A + c_B} \quad \text{E3.9}$$

use equations E3.3 and E3.4 to obtain:

$$p = \frac{\frac{j_o}{D_B} + M \nabla c_A - \nabla c_A}{M c_A + c_o - c_A} \quad \text{E3.10}$$

to obtain the equation in terms of p_A only, use the definition for M again and simplify equation E3.10 to obtain:

$$\frac{eE}{fkT} = \frac{(M-1) \nabla c_A + \frac{M j_o}{D_A}}{c_A (M-1) + c_o} \quad \text{E3.11}$$

Take equation E3.11 and plug it into equation E3.1 to obtain:

$$j_A = -D_A \nabla c_A + c_A D_A \frac{(M-1) \nabla c_A + \frac{M j_o}{D_A}}{c_A (M-1) + c_o} \quad \text{E3.12}$$

Simplifying gives:

$$j_A = \frac{-D_A c_o \nabla c_A + M c_A j_o}{c_A (M-1) + c_o} \quad \text{E3.13}$$

This is now the flux with the dopant ion as the only variable. The self diffusion constant will be set as well as the total ionic flux and the total concentration. Therefore to obtain the change in concentration of c_A as a function of time Fick's second law is used as follows:

$$J = \frac{-D\nabla C + MCJ_o}{C(M-1)+1} \quad \text{E3.15}$$

At this point it is useful to simplify the terms in equation E3.13 by using the following substitutions, $J = j_A/c_o$, $J_o = j_o/c_o$ and $C = c_A/c_o$. This will produce relative fluxes and a relative concentration. Using these in equation E3.14 will give the following:

$$\frac{\partial C}{\partial t} = \frac{D\nabla^2 C}{C(M-1)+1} - \frac{D(M-1)(\nabla C)^2 + MJ_o \cdot \nabla C}{[C(M-1)+1]^2} \quad \text{E3.16}$$

This equation can be expanded as follows:

$$\frac{\partial c_A}{\partial t} = -\nabla \cdot j_A \quad \text{E3.14}$$

This equation can be solved numerically using a finite difference method (see appendix A3.1 for details). Appendix A3.2 is a copy of the Fortran program written to solve for the concentration. Figure 3.2 is a plot of the self diffusion coefficient with respect to time. Each individual plot is a separate time. The diffusion rate has been set at 0.002 $\mu\text{m}^2/\text{sec}$ and the ratio of self diffusion coefficient has been set at 1.0 and the times vary from 20 seconds to 100 seconds in steps of 20 seconds.

A plot holding the time constant and changing the ratio of self diffusion coefficient is shown in Figure 3.3. The ratio is changed from 0.2 to 1.0 in steps of 0.2. As can be

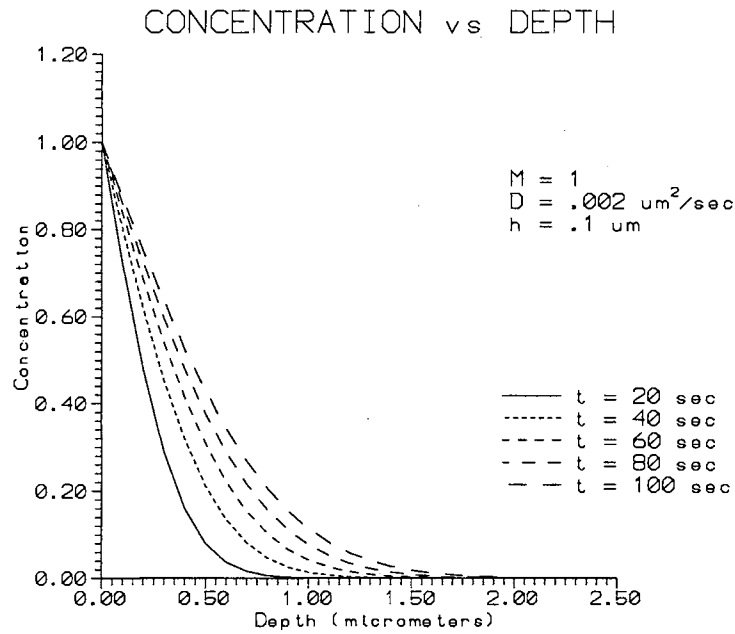


Figure 3.2. Theoretical refractive index profiles for ion-exchange. This is for a constant self diffusion coefficient, ratio of self diffusion coefficient and thickness. The time was varied to obtain the different plots.

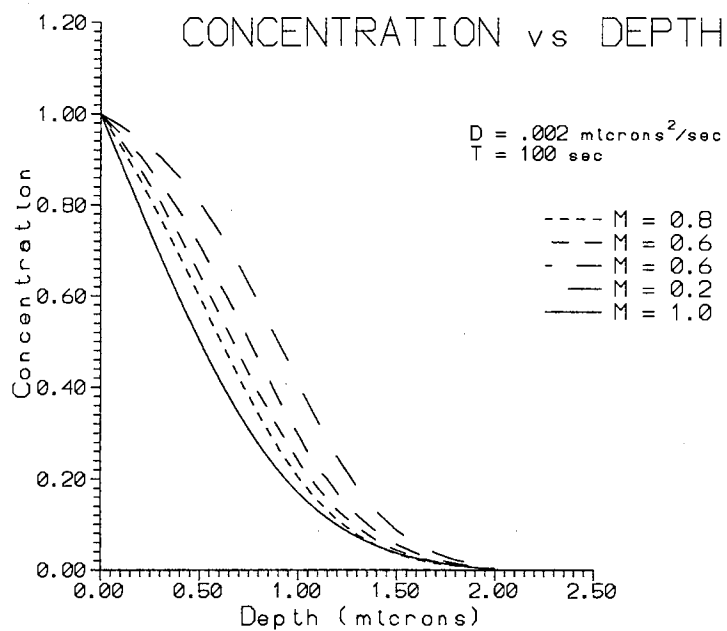


Figure 3.3. Theoretical refractive index profiles for ion-exchange. This is for a constant self diffusion coefficient, waveguide thickness and time. The self diffusion coefficient ratio was varied.

seen, there appears to be very little affect when M is close to 1.0. However, for small values of M the plot departs significantly from the linear solution. The M which is being changed here is the ratio of the dopant ions going into the glass with respect to the original ions leaving the glass. This implies that for $M = 0.1$ there will be more substrate ions moving out of the substrate than salt bath than ions diffusing inward. Salt bath ions, which are larger, diffusing into the substrate will create stress, adding to the change of refractive index.

Buried waveguides

The ion-exchange process is for a single ion-exchange. It is possible to do a second ion-exchange process and remove the ions diffused the first time. This technique produces a buried waveguide, thus reducing surface scattering and lowering the loss of the waveguide. The process is the same as discussed above except the salt bath is changed to contain the same ion which is pulled out the first time. If just a small amount of original exchanged ions are replaced, a buried waveguide will result. This second ion-exchange with the host ion is called back diffusion. Back diffusion has several positive results. Two glasses with similar characteristics will not necessarily respond the same way to the back diffusing process, and not all glass is capable of back diffusing. One may back diffuse successfully and the other may ruin the surface of the glass. It is possible for chemical degradation of the surface to occur during the back diffusion process.

Applying an electric field in conjunction with the thermal process of ion-exchange creates the third refractive index profile as shown in Figure 2.4. A fourth profile is the buried waveguide. The buried waveguide is made by controlling the diffusing ions. This is done by removing the salt bath ions which are being diffused into the substrate and applying heat and an electric field. This is done after an initial ion-exchange period. The diffused ions are then be pushed deeper into the substrate burying the waveguide. Turn off the electric field while still applying the heat, this is called annealing.⁴⁰⁻⁴³ A smoothing or rounding effect will take place. This demonstrates a more complete control over the profile.

CHAPTER IV

FABRICATION PROCESS

The fabrication process for channel waveguides consists of a masking process for fabricating a specific channel width, an ion-exchange process to raise the refractive index and a polishing process to reduce scattering for input and output coupling. This chapter provides the necessary information to fabricate a channel waveguide in a glass substrate.

The ion-exchange process, as described in chapter III, is done by taking a potassium salt bath, KNO_3 , and heating it until it melts. The melting point for pure KNO_3 is 335°C . The substrate is placed in the oven and allowed to heat up at the same rate as the KNO_3 . Once the KNO_3 has melted, the substrate is placed in the salt bath for a specified period of time. After that allotted time the substrate is removed and cooled. A thick residual layer of KNO_3 is left on the substrate which rinses away with water. The substrate will physically appear unchanged, however x-ray analysis shows a change in the elemental make up of the glass.

Masking Process

The masking process used in the laboratory for patterning, is done with photoresist and aluminum evaporation. Before this can take place the sample must be taken through a preparation process. The preparation process accomplishes two things, the first is simply to make sure the substrate is clean. The second however, is to ensure the

photoresist will adhere well to the sample. The cleaning process consists of two steps. The first is to clean the sample with soap and water. (It is important to note that the soap must be oil and acid free. If it is not it will leave a thin residue prohibiting good adhesion. The water must be de-ionized or it will also leave a residue prohibiting good adhesion.) A Q-tip is used to scrub the sample's surface and remove any particles which will not simply spray off with a stream of water. The second step is to place the sample in an ultrasonic cleaner with acetone and then methanol. This is left to vibrate for at least five minutes in each solution.

Sample handling is critical to preserve the preparation. The sample is carefully handled with rubber gloves to protect the substrate from oil. The sample is blown dry with pure nitrogen to remove any excess moisture. It does however still contain a certain amount of moisture which will cause lifting of photoresist if it is not removed. This remaining moisture is removed by heating the glass substrate. Consideration must be taken when selecting the temperature as the glass has a transformation temperature that varies for different glasses. Since most glasses have a transformation temperature above 250 °C, 200 °C is used. The sample is left on the hot plate for thirty minutes. The times used to vibrate and heat the sample for consistent results were obtained by trial and error.

Once the sample has been prepared, Hexamethyldisilane (HMDS) is spread with a spin coater. HMDS is used for better photoresist adhesion. It is spun until it evaporates completely leaving the sample ready for photoresist. All of the procedures mentioned

above are done in a clean room to prevent dust and contamination from regathering on the substrate. Photoresist is light sensitive and must be used in darkroom conditions. It is more sensitive in the UV range and that is the source which is used. A thickness of 2 micrometers using Shipley S1400-31 produced the best results for lifting off the aluminum which was 1.5 micrometers thick.

The photoresist has a limited shelf life, and if not used within that time, the results are not reproducible. Similarly, the HMDS has a shelf life, and if not applied when fresh the photoresist will not adhere to the HMDS coated substrate. The spin time is one of the determining factors in the thickness of the photoresist. The sample must be spun long enough to provide a smooth surface but not so long that the required thickness diminishes. Spin times were varied until optimum results were obtained.

Initially the sample with the thin layer of photoresist was immediately placed under the UV lamp with a mask containing a specified pattern. The UV lamp has 350 mW/cm² of power at 405 nm. The amount of time the sample was left under the lamp was also varied until an optimum result was achieved. The sample was then placed in a developer, Microposist 351, for a specified period of time. The time was again varied until the optimum results were obtained. The desired result was to have two micrometer thick ridges of varying widths. Expected results were inconsistent. It was discovered that solvents in the photoresist create a very unstable break-down time when exposed to UV light. When a large amount of solvent is left in the sample the process requires very little

light exposure. If there is very little solvent left in the photoresist then the process requires additional light exposure. To correct this inconsistency the solvents are driven off by applying heat. This is called a soft bake process. The photoresist did not respond well when it became too dry. Some moisture had to be placed back in the photoresist. This was done with a desiccator. The times the sample spent in the heat and the desiccator were varied until optimum results were obtained. Figure 4.1 shows photographs, taken with an SEM, of photoresist ridges taken on two separate occasions.

The ridges made from the photoresist should be flat on the top with flat sides. The first photograph shows severe bumps and rounding on the sides. Another significant point which cannot be seen by this photograph is the discontinuity of the ridge. The strip breaks in spots and in certain parts of the strip the ridge simply does not exist. The second photograph displays a flat top and flat sides. It is also a continuous strip from one end of the substrate to the other. A table listing the necessary events and times to obtain optimum results is given in table 4.1. This procedure will ensure consistent results each time because it controls the items which affect the final outcome. Both the temperature and the humidity affect the final outcome and must be considered. The problems of temperature and humidity are taken care of by heating the photoresist and afterwards placing the sample in a desiccator.

Once the photoresist has been successfully applied the sample is coated with aluminum using an Edwards E306A vacuum coater. It is important that enough aluminum

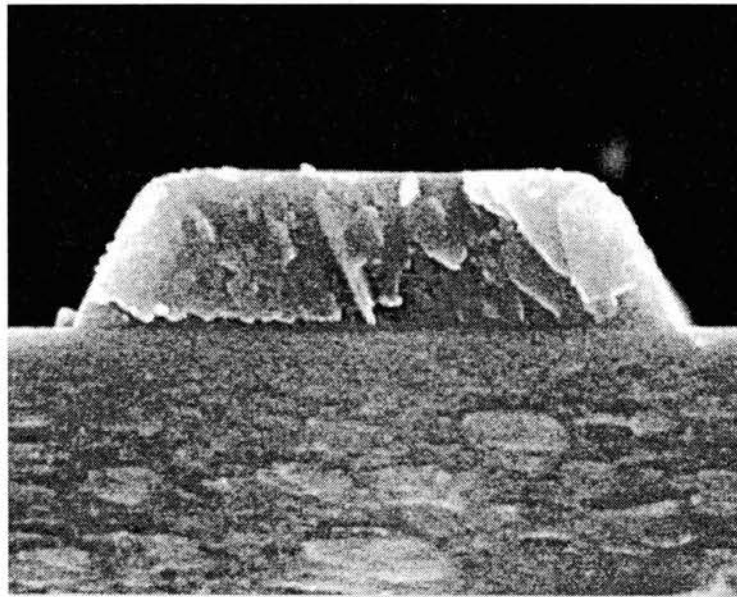
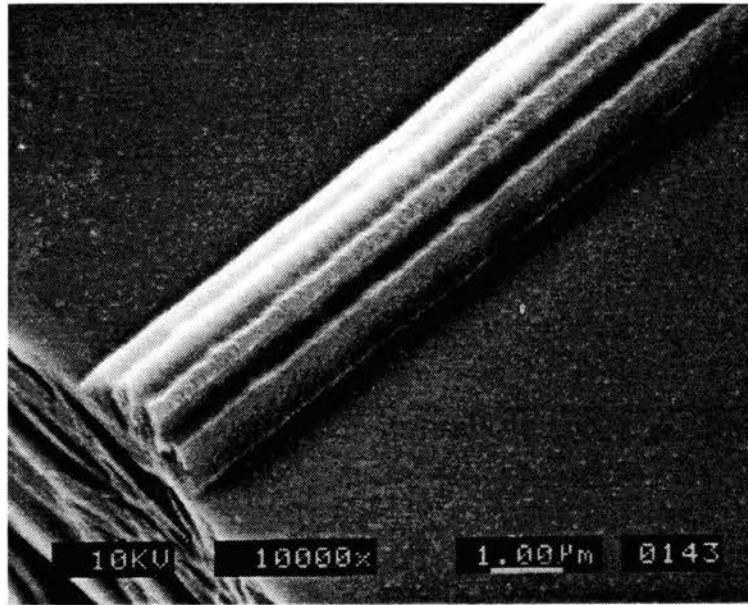


Figure 4.1. Photoresist ridges taken with an SEM. The first photograph displays rounded edges. The second photograph displays a flat top and is continuous.

EVENT	TIME	TEMP	RPM
Ultra Sonic Cleaner			
Acetone	5 min		
Methenol	5 min		
Pre-Bake	30 min	200 C	
Spin HMDS	60 sec		3500
Spin Resist	60 sec		3500
Soft Bake	30 min	90 C	
Desiccate	10 min		
Expose	35 sec		
Develop	60 sec		

Table 4.1. Specific times and events to produce consistent photoresist ridges using Shipley 1400-31 positive photoresist.

is coated to block the ion-exchange in areas which are not to be exchanged. At this point in time there is no exact amount, however it was discovered that if the aluminum is too thin the ion-exchange will diffuse through the mask. The diffusion rate through the aluminum is not as fast as the uncoated diffusion rate but will create a waveguide in an undesired region. Initially the process used was to apply approximately 200 nm of aluminum. This allowed the aluminum on the photoresist to lift off without difficulty leaving strips of aluminum on the substrate. The final result was thin planar guides coupled with larger channel waveguides. A good separation of waveguides was not achieved. A thicker coat of aluminum was the solution, but this in turn created a problem with the stripping process. The problem was solved by coating the substrate and photoresist with a one and a half micron thick aluminum layer. This completely covered the sample and the photoresist. The sample was then etched in phosphoric acid and heated. A layer of aluminum was released, exposing the sides of the photoresist ridges. This process is demonstrated in Figure 4.2.

The sample can then be placed in acetone which will wash away the photoresist, taking with it further strips of aluminum. The final result is a good adhesion of aluminum to the substrate in strips of specified width and distance apart. This is also a critical issue since the ion exchange will not only penetrate the glass vertically, but will also move horizontally. It is possible to place the exposed or uncoated strips too close together which promotes energy leakage from one waveguide to another. The exact minimum distance between the waveguides to avoid leakage is not known. A safe

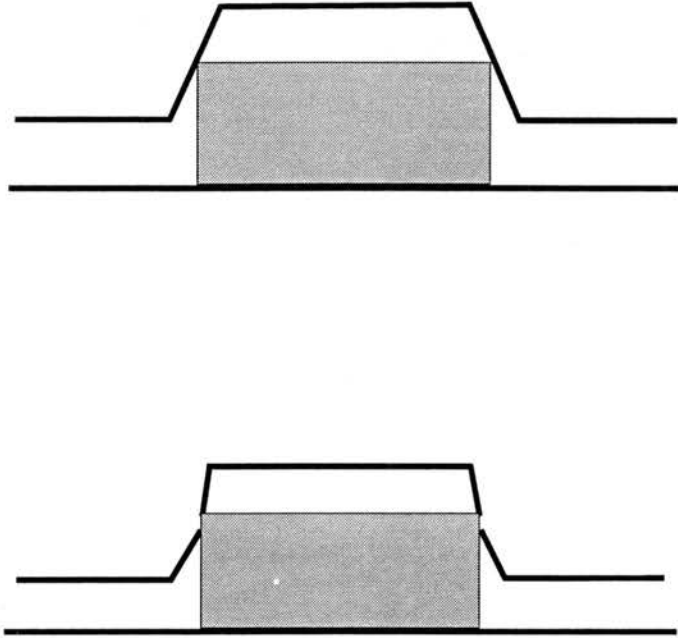


Figure 4.2. Photoresist shown in the solid grey is coated with aluminum as shown on the top sketch. After the etching process the photoresist is exposed on the upper edge of each side.

distance between the waveguides can be estimated using the coupling equations. The waveguides were then spread a considerable distance farther apart to ensure independent guiding of light. The lines in the mask range from one micron to as many as two hundred microns. A copy of the mask is shown in Figure 4.3.

The picture in Figure 4.3 displays just a few of the total lines contained in the mask. The mask contains the following line widths, all in microns:

1, 2, 3, 4, 5, 6, 7, 8, 9, 10, 15, 20, 30, 40, 50, 75, 100, 200

This demonstrated broad range allows for a wide variety of tests with one mask.

An overview of the fabrication process can best be described with a step by step procedure diagram. Once the mask is in place, thermal ion exchange can be done by placing the substrate into a salt bath and heating. Figure 4.4 displays an outline procedure for the fabrication of a channel waveguide using ion-exchange.

Polishing

There are three main methods for coupling light into waveguides. A grating can be placed on the waveguide, and light incident at just the right angle will launch light into the guide. A prism can be pressed against the waveguide and light entering the prism at the precise angle will also couple into the waveguide. These methods are useful, but can be complicated to set up. Using these methods to couple into channel waveguides is equally as complicated and inefficient. End fire coupling is used to overcome many of

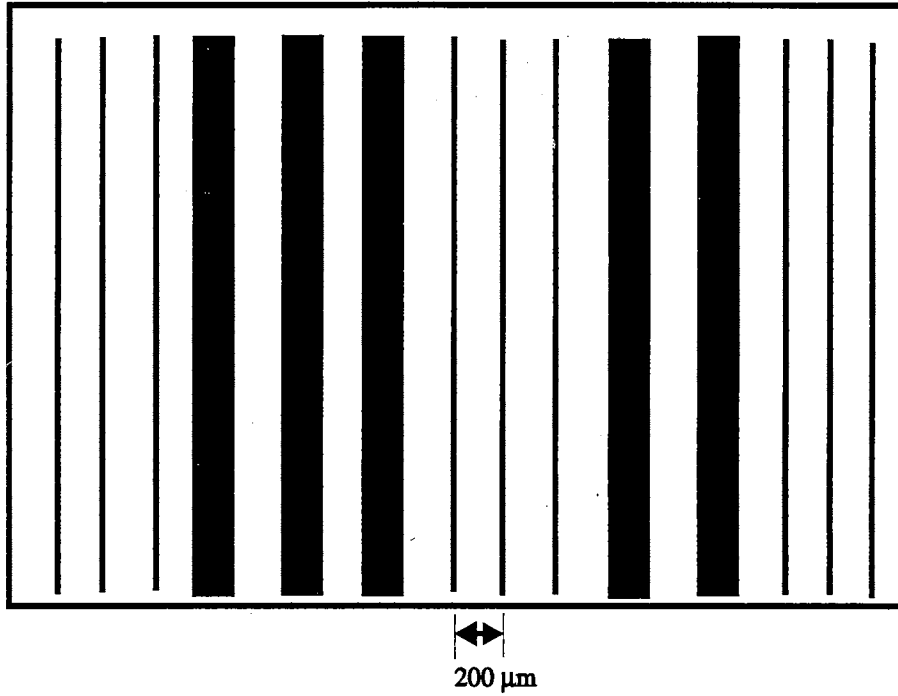


Figure 4.3. Mask used for positive photoresist patterning. Each dark strip is a metal cover to prohibit light exposure directly beneath the mask.

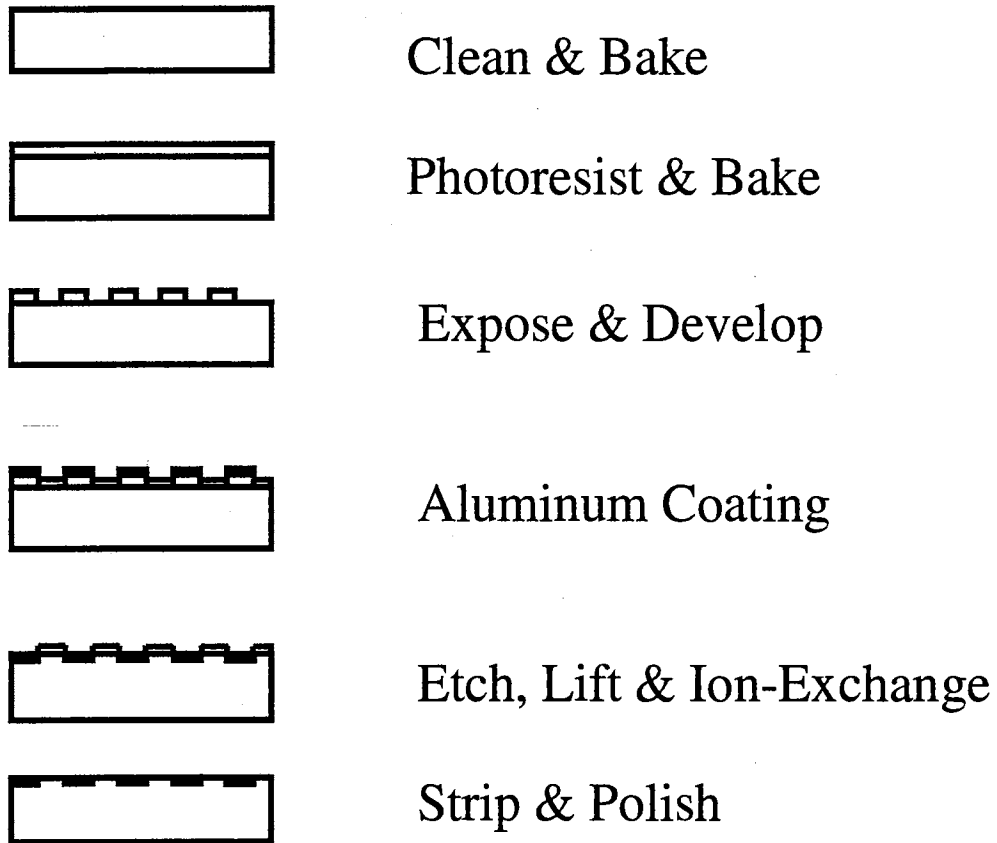


Figure 4.4. Fabrication process to make channel waveguides with ion-exchange.

these barriers. End fire coupling can be used to couple into fibers and then butt the fiber against the channel waveguide. In order to get the maximum coupling efficiency the ends of the waveguide must be polished. If the end has a good polish then the major loss will be profile mismatch and Fresnel reflections. Scattering due to surface roughness can be reduced significantly. Two of these three methods are used in the laboratory and the setup for these is shown in Figure 4.5.

Initially polishing was done by taking the sample and placing it in an epoxy holder. The dry epoxy held the sample in place during the polishing. Removing the sample from the epoxy is both difficult and frequently harsh on the sample. Epoxy forms a very close bond with the glass. Any rounding due to polishing should not affect the glass, just the edge of the large epoxy holder. The polished glass appeared to have a very smooth surface on it and endfire coupling was accomplished successfully. Epoxy grinds and polishes at a much faster rate than the glass, so the glass edges did round. The rounding effect can be seen by taking the sample and placing it under an interferometric scope. The fringes in the scope will display the contour of the surface being observed. Figure 4.6 displays two photographs of the fringes created from two pieces of glass polished together. The first set was held in an epoxy holder. The severe rounding is obvious from the fringes curving downward to show a gap between the two pieces of glass.

This problem is solved by taking the second piece of glass and pressing it against

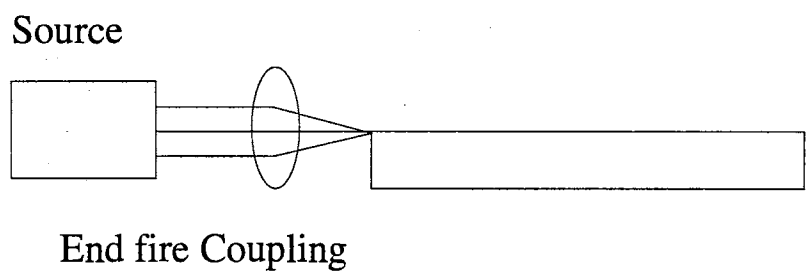
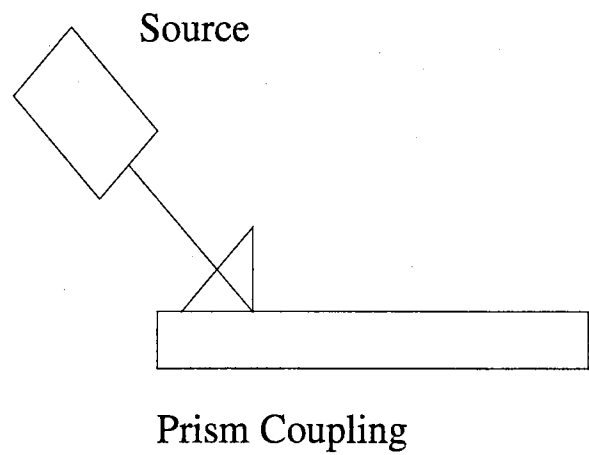


Figure 5.4. Setup for both prism coupling and endfire coupling into optical waveguides.

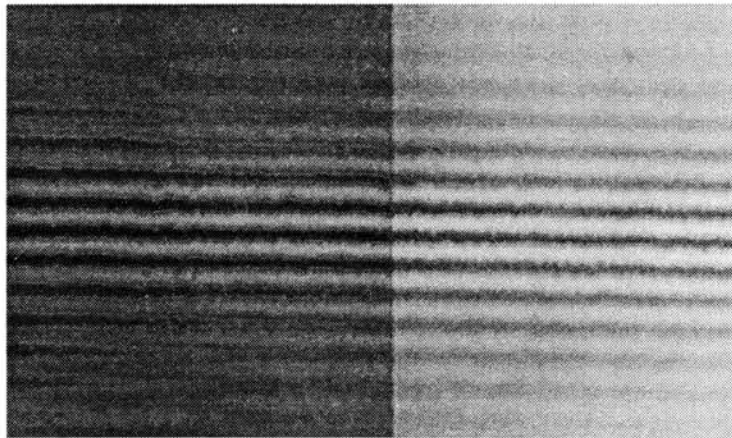
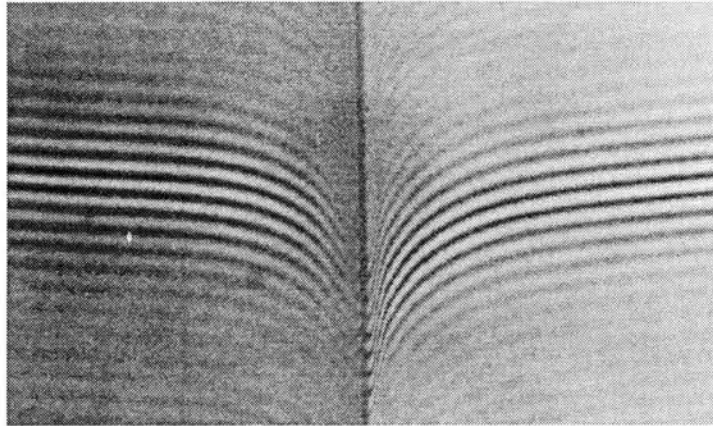


Figure 4.6. Fringes displaying the rounding effect due to two pieces of glass held in an epoxy holder for polishing are shown in top photograph. The bottom photograph displays the results when the two pieces of glass are pressed tightly together.

the substrate until optical contact is achieved. A thin strip of index matching glue is placed on each side of the two pieces. When the glue has dried the sample is then sandwiched between layers of glass and held together in a plexy glass holder. Wax is used to keep all of the pieces in place and also used as a cushion for extra stresses upon the glass. The sample then goes through the normal grinding and polishing stages. The sample with highly polished ends, can now easily be taken out of the holder . The second photograph in Figure 4.6 shows the improvement achieved with the new technique.

Endfire coupling can now be done with better efficiency and reliability. Coupling efficiency to and from fibers will also improve with this polishing technique. Photographs of prism coupling and endfire coupling are shown in Figure 4.7. The first picture shows light being coupled into a planar waveguide via a prism. The prism was covered in the photograph, the streak displayed is confined in one dimension. Endfire coupling is demonstrated in the second photograph, using a channel waveguide.

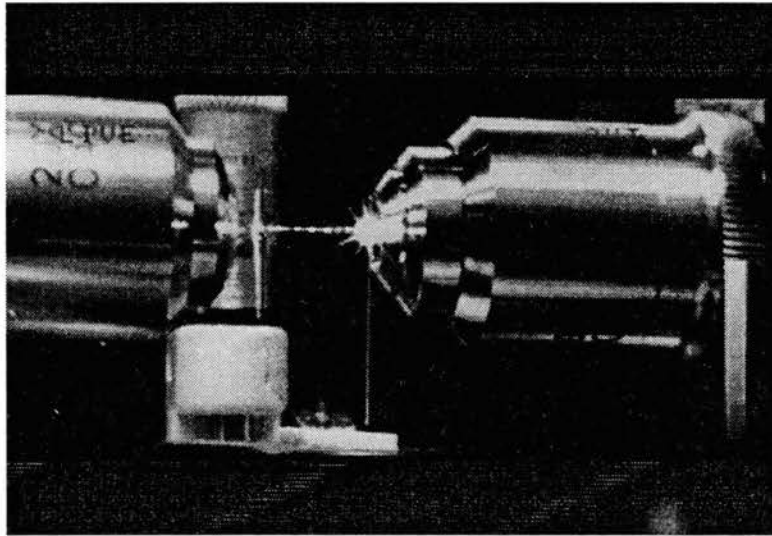
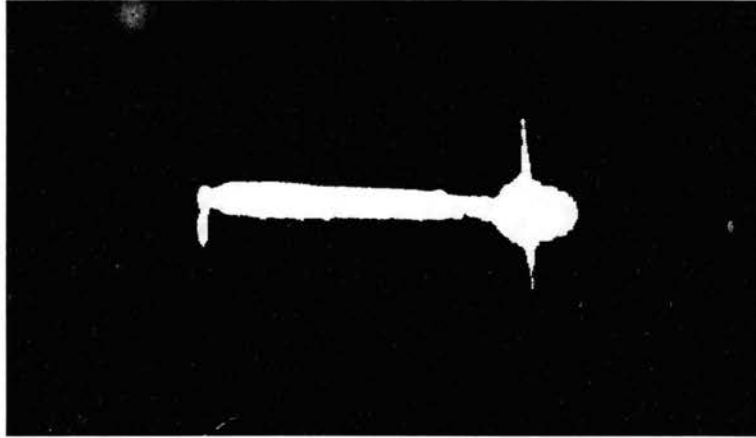


Figure 4.7. Photographs of light being coupled in waveguides via prism coupling and endfire coupling.

CHAPTER V

CHARACTERIZATION OF OPTICAL WAVEGUIDES

Characterization techniques including observing waveguide profiles, measuring the diffusion coefficient and noting waveguide loss are necessary for designing specific optical waveguides. The contribution of each of these methods provides the necessary information for controlling and designing channel waveguides. Shaping the profile of the waveguide for specific applications requires a specific technique to measure that profile. Currently, several techniques such as the inverse WKB¹², backscattered x-rays²¹, Secondary Ion Mass Spectroscopy (SIMS)⁹, microprobe analysis²⁴ and far field diffraction patterns are used to measure the concentration profile. The WKB method requires prior knowledge of the profile of the waveguide. It is not self-sufficient for direct observation of the concentration profile of an ion-exchanged waveguide. Backscatter is a non-destructive method that is only qualitative and it is limited to observation of only the heavier elements such as silver. SIMS is a destructive method which is time consuming and requires expensive equipment for an estimate of the concentration profile. While electron microprobe also requires expensive equipment which is relatively easy to find, it is a technique which has the potential for measuring concentration profiles of atoms as small as boron. It has been used qualitatively. We have extended this technique in order to make quantitative measurements of concentrations and concentration profiles. The far field diffraction technique is used to observe directly the intensity profile of the waveguide.

This chapter describes in detail the electron microprobe technique where this method is used to measure the interaction volume and the concentration profile of waveguides made by ion-exchange with potassium. A technique for directly measuring the number of modes in a waveguide is also described. A new technique to measure waveguide loss is described and demonstrated.

Electron Microprobe Analysis

As described in Chapter I, microprobe analysis has been used in a limited fashion to study optical waveguides. Electron microprobe analysis of optical waveguides made by silver ion-exchange has been demonstrated by Ramaswamy and et al.¹² Silver (atomic weight = 107.87) is a heavy ion which is easily detected by an x-ray detector. Analyzing optical waveguides which have been ion-exchanged with potassium presents a challenge since potassium (atomic weight = 39.10) is a much lighter element. Electron microprobe analysis of silver-exchanged waveguides has been demonstrated for waveguides with a depth of at least eight microns. Observing single mode waveguides made by potassium ion-exchange to depths on the order of eight micrometers thick has not been done since the spatial resolution of electron microprobe is low in comparison with the depth of the waveguide. This has prohibited quantitative measurements of the concentration profile and accurate diffusion coefficient measurements as well. A technique to allow the direct observation of single-mode waveguides made from potassium ion-exchange is described below.

Electron microprobe analysis requires the use of a Scanning Electron Microscope (SEM). The SEM emits an electron beam which strikes the sample surface. There is enough energy in this beam to knock electrons out of the inner shells of the atoms embedded in the glass surface. When an electron is removed from the inner shell an outer shell electron decays to fill the vacancy left by that inner shell electron. The decaying electron emits an x-ray photon which is characteristic of the energy difference between the two levels. This is illustrated in Figure 5.1. Each atom has a characteristic x-ray energy spectrum which identifies that atom. The energy for each atom is on the order of thousands of electron volts. Each time an x-ray is emitted it travels in a random direction through the SEM chamber. An x-ray detector made from a silicon-lithium crystal receives some of the emitted x-rays. Each one received creates a charge on the crystal. The charge is then converted to a small voltage in the pre-amplifier stage. This voltage is sent to a second amplifier and multi-channel analyzer. The signal is then processed by a computer to determine which element the signal most closely fits. The pulse processor has a limited number of pulses it can process in a specified time period. In the event the processor is full, the analyzer goes into a dead-time state. During the dead-time the pulse processor sends the accumulated information to the computer. Once the pulse processor is empty it begins gathering more x-rays. Not all x-rays emitted by the sample are received by the detector, and not all x-rays received by the detector are processed by the pulse processor. To obtain a good statistical sample, several thousand verified responses indicating a specific element must be processed through the x-ray system. The output from the computer is displayed as a spectral response, where each element is represented

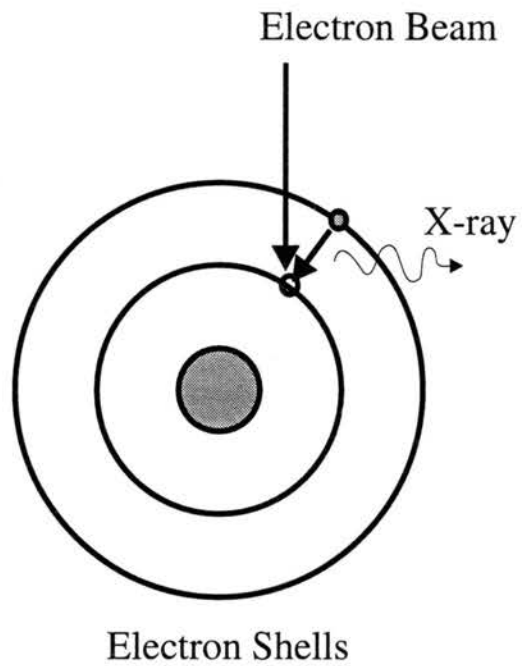


Figure 5.1. A model of a nucleus with the surrounding electron shells. An electron beam with enough energy will remove an inner shell electron. An outer shell electron will fill the hole thus releasing x-ray radiation.

by a specified place on the spectrum. A typical x-ray spectrum is shown in Figure 5.2.

The accuracy of the microprobe contributes to the over-all effectiveness of this technique. A Voyager light element detector by Noran was the x-ray analyzer used. Noran states the accuracy of their detector is approximately 0.5% by compositional weight. For example 20% potassium should be read as $20\% \pm 0.5\%$. This is for heavier elements such as sodium or silver. Lighter elements such as carbon require a reference for high-accuracy detection. A test was done on a piece of glass with a known composition. The glass tested was Corning 2947, a silicate base glass known as soda lime glass. Soda lime glass contains silicate, sodium, calcium, magnesium and aluminum. The x-ray analysis system has the option of manually identifying known elements when greater accuracy is required. Examining optical waveguides can be done by identifying the elements in advance since the glass type is typically known and the ion to be exchanged is also known. The elements were keyed into the system and a quantitative analysis was performed on the Corning 2947 glass. This was compared to the manufacturers data sheet accurately shown in Table 5.1. As can be seen from the table the results are good and fall within the error stated by the manufacturer of the microprobe system. This data was obtained by setting the live-time to 120 seconds, the accelerating voltage to 15 KV and the magnification to 2000x. If the accelerating voltage is set for less than 15 KV the results become noisy and inconsistent.

Table 5.1 displays results from a large area scan, seventy five microns by seventy

EDS SPECTRUM OF GLASS

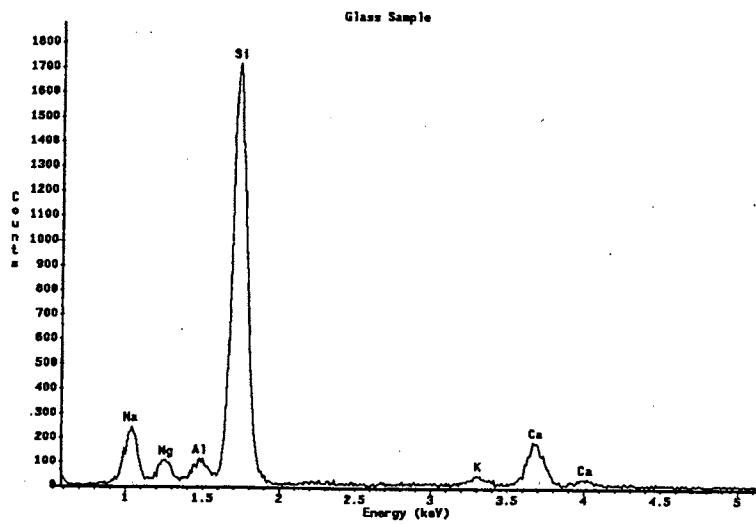


Figure 5.2. A spectral output for an EDS system. Each peak is a specified element where the relative concentration is related to the height of the peak.

MATERIAL	EDS	MANUFACTURE
SiO ₂	73.4 %	73 %
Na ₂ O	13.3 %	14 %
Al ₂ O ₃	2.2 %	2 %
MgO	4.4 %	4 %
CaO	6.7 %	7 %

Table 5.1. Comparison of manufacturers data sheet on Corning 2947 with EDS quantitative output. EDS was set at 15 KV accelerating voltage, 2500 magnification and a live time of 45 seconds.

five microns. This can be taken one step further and a spot on the glass sample can be analyzed in the same manner. The electron beam is approximately 200 Å for an Amray 1600 SEM. This would allow a high resolution line scan to be done on waveguides with a depth of two to ten microns. The spot size is not the determining factor in the spatial resolution of microprobe analysis. The electrons scatter inside the glass sample to emit x-rays which are emitted from a region approximately a few microns in size. This region is called the interaction volume. The volume size depends on the electron beam energy and composition of the sample. The shape and the depth of the penetration depends upon the accelerating voltage and the material being examined. Richards determined the shape and the size by examining a polymer material.⁴⁷ After the electron beam struck the sample, the polymer was chemically etched away while photographs were taken of each layer as it was etched away. From the photographs it was obvious the electron beam impacted the strongest in the center of the polymer and decayed outward. This decay could be represented using some kind of exponential or gaussian shape. The interaction volume is represented in Figure 5.3.

With an interaction volume of three microns, obtaining information from a six micron deep waveguide would provide two points for the profile. Over sampling can be done by collecting data from many more points from the same line than just two. This gives an averaging effect which produces accurate information from each point obtained. Reducing the interaction volume to one micron by reducing the accelerating voltage allows for higher resolution which adds to the accuracy of the averaging effect. The

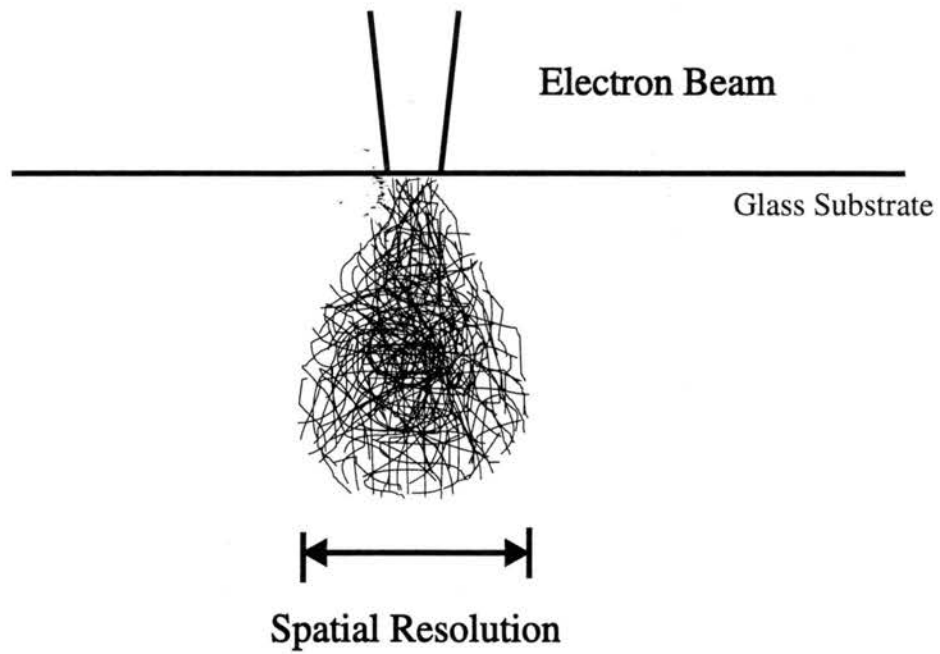


Figure 5.3. Interaction volume for X-Ray analysis. The higher the accelerating voltage the larger the diameter.

interaction volume spreads the end of the profile since x-rays are detected from the tail of the gaussian-shaped detection area. This problem was solved by taking the solution to the diffusion equations discussed in chapter III and convolving them with a gaussian function. The mathematical analysis for this is discussed in Appendix A5.1. It is expected the solution for the diffusion equations, erfc, will appear with rounded edges and spread out from the original solution. The results for this are shown in Figure 5.4. This is indeed what happens, which implies that if enough information can be obtained from the experimental data then accurate diffusion coefficients can be obtained.

The aforementioned authors, Ramaswamy and DeBernardi, have used microprobe to analyze optical waveguides with depths in the range of twenty to sixty microns.^{23,26} This will provide a good estimate of the diffusion profile since the interaction volume will be small compared to the overall depth of the waveguide. This still does not eliminate the problem on the edge of the sample and does not allow direct observation of shallow depth waveguides. To eliminate the edge problem a piece of Corning 2947 glass was ion-exchanged for a specified period of time. A piece of Corning 2947 was optically contacted to an ion-exchanged sample. The end face where the two pieces of glass meet were then polished to obtain a smooth, continuous surface. This provides a homogeneous line scan with the microprobe. The only effect which is seen in the line scan is due to the exchanged ion entering the glass. A step size of 0.02 μm has been used with accurate information for each point. This evidence leads to the conclusion that over-sampling coupled with deconvolution permits higher resolution even for single mode waveguides

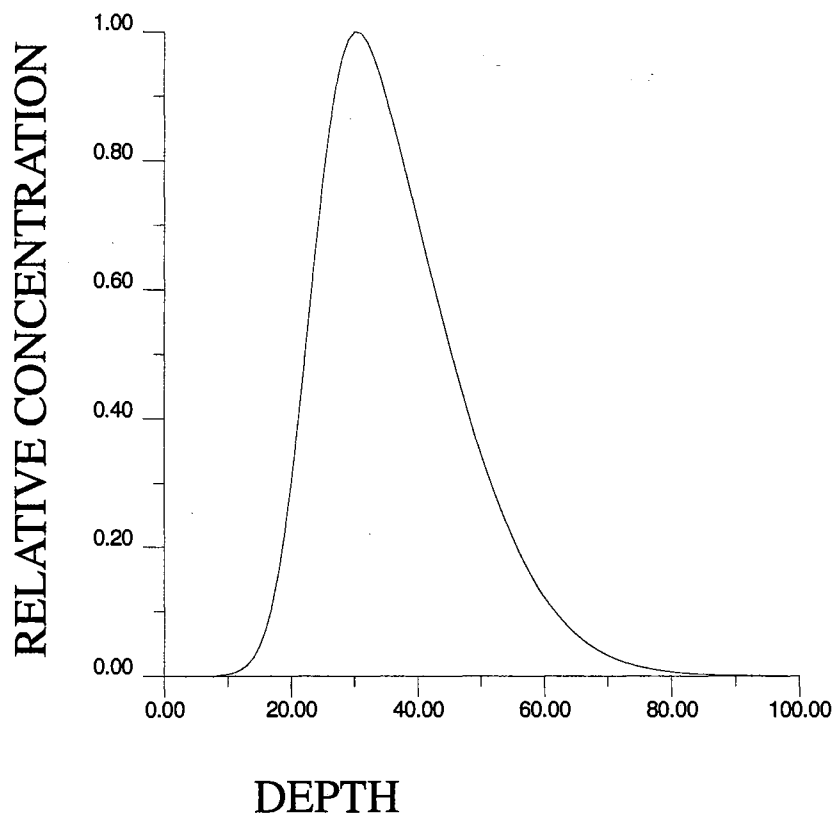


Figure 5.4. Analytical solution for the convolution of the complementary error function and a gaussian function.

with depths as small as six micrometers.

The same concept can be applied to estimate the interaction volume using the above sample preparation technique . Two pieces of dis-similar glass were optically contacted. The two samples that were used were Corning 2947 and BK-7. The Corning contains approximately 7% calcium by weight and the BK-7 has no calcium. A line scan was done using a live time of 180 seconds, an accelerating voltage of 15 KV and a magnification of 2000X. The step size used was 0.1 μm . The total length of the scan was 20 μm . The results were compared to the theoretical model shown in Appendix A5.2. A least squares fitting routine was used to obtain a gaussian width. The fitted data displayed a Full Width Half Maximum (FWHM) of approximately one micron as shown in Figure 5.5. A comparison was made using the slope of the transition for the slope in the equations shown in Appendix A5.2, the FWHM for this technique was approximately one micron as well.

The diffusion coefficient and the ratio of the diffusion coefficient was estimated by taking four pieces of glass and ion-exchanging these pieces for fifteen minutes, one hour, three hours and eight hours. Line scans were then performed and the data acquired was used in the least squares fitting routine. This was done for each piece ion-exchanged. The first piece was scanned twice, the second piece was scanned four times, the third piece was scanned six times and the fourth piece was scanned six times. A table summarizing the results along with the SEM, x-ray settings are shown in Table 5.2. The

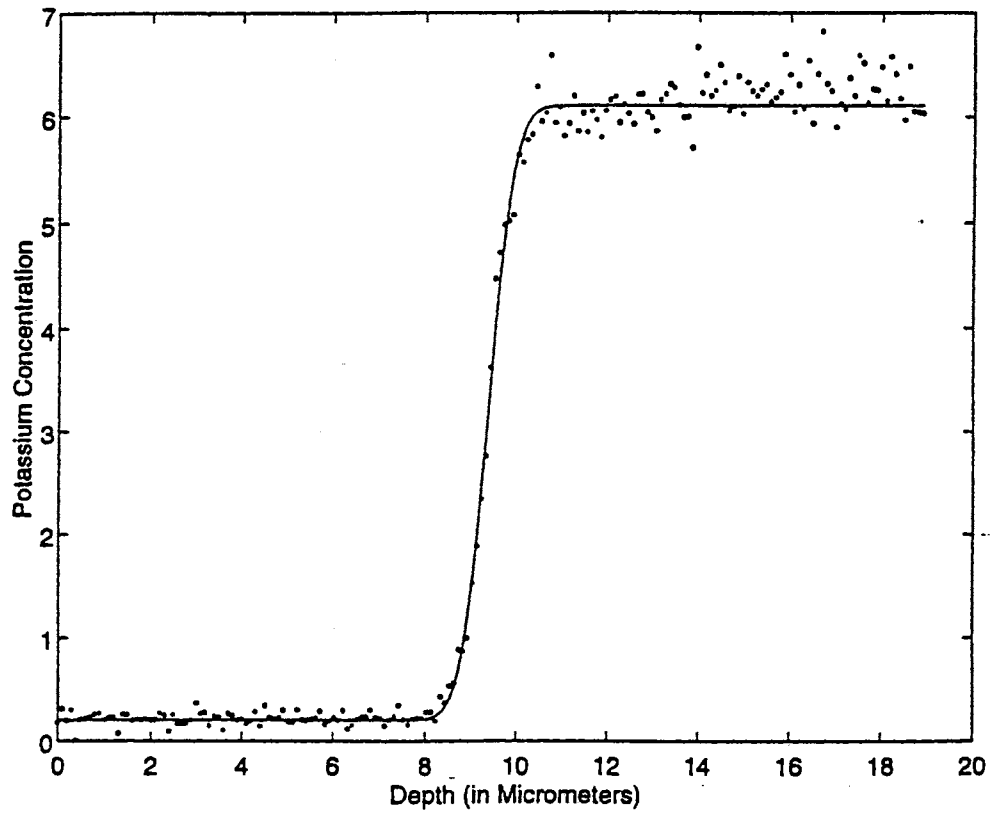


Figure 5.5. Curve fit of x-ray linescan and theoretical model of a step function convolved with a gaussian function.

0.25 HOURS ION-EXCHANGE

D = 4.08 AVG = 3.75
D = 3.47 STD = 0.31

1.00 HOURS ION-EXCHANGE

D = 3.10
D = 3.48 AVG = 3.30
D = 3.08 STD = 0.21
D = 3.52

3.00 HOURS ION-EXCHANGE

D = 2.35
D = 2.49
D = 2.48 AVG = 2.38
D = 2.44 STD = 0.11
D = 2.16
D = 2.39

8.00 HOURS ION-EXCHANGE

D = 1.67
D = 1.82
D = 1.51
D = 1.19 AVG = 1.56
D = 1.59 STD = 0.19
D = 1.74
D = 1.55
D = 1.39

SEM SETTINGS:

Accel Volt => 15 KV
Beam current => 50 uA
Magnification => 2500
Working Dist => 24 mm

X-RAY SETTINGS:

Livetime => 120 sec
Deadtime => 25%
Magnification => 2500
Accel Volt => 15 KV

Table 5.2. Corning 2947 ion-exchanged for four different times. Curve fitting was then performed and the diffusion coefficient for each plot was found. Both SEM and X-ray settings are given.

times were taken and plotted against the diffusion coefficients, shown in Figure 5.6. Previous literature concludes the diffusion coefficient is constant for a specified piece of glass at a constant ion-exchange temperature. As noted earlier these conclusions come from long ion-exchange times or waveguides with deep concentration profiles. The results obtained for short ion-exchange times or shallow waveguides indicate the diffusion coefficient is higher for shorter times. As the time is extended the diffusion coefficient drops until a saturation point is reached and the diffusion coefficient becomes constant. One of the fits, four hour exchange, is shown in Figure 5.7. As the plot demonstrates and the results in the table show, the technique is consistent and accurate.

Malone has stated that electron microprobe is only for qualitative analysis. We have shown that this technique was used successfully to examine planar waveguides quantitatively and produced reliable results. This technique has also been taken one step further and used as a qualitative tool for examining channel waveguides. This is done by taking a channel waveguide and scanning in a matrix format. Once the channel waveguide is located, a matrix of points is set up to obtain quantitative results concerning the potassium concentration. The information provided is certainly an accurate profile of the channel waveguide. The theoretical model was not, however developed for comparison with experimental data. To demonstrate what a valuable tool this can be for examining channel waveguides, Figure 5.8 demonstrates a two dimensional x-ray matrix showing potassium concentration vs. depth and width. A second two dimensional plot, shown in Figure 5.9, demonstrates the same idea when a dip in the waveguide is present.

Time vs. Diffusion Coefficient

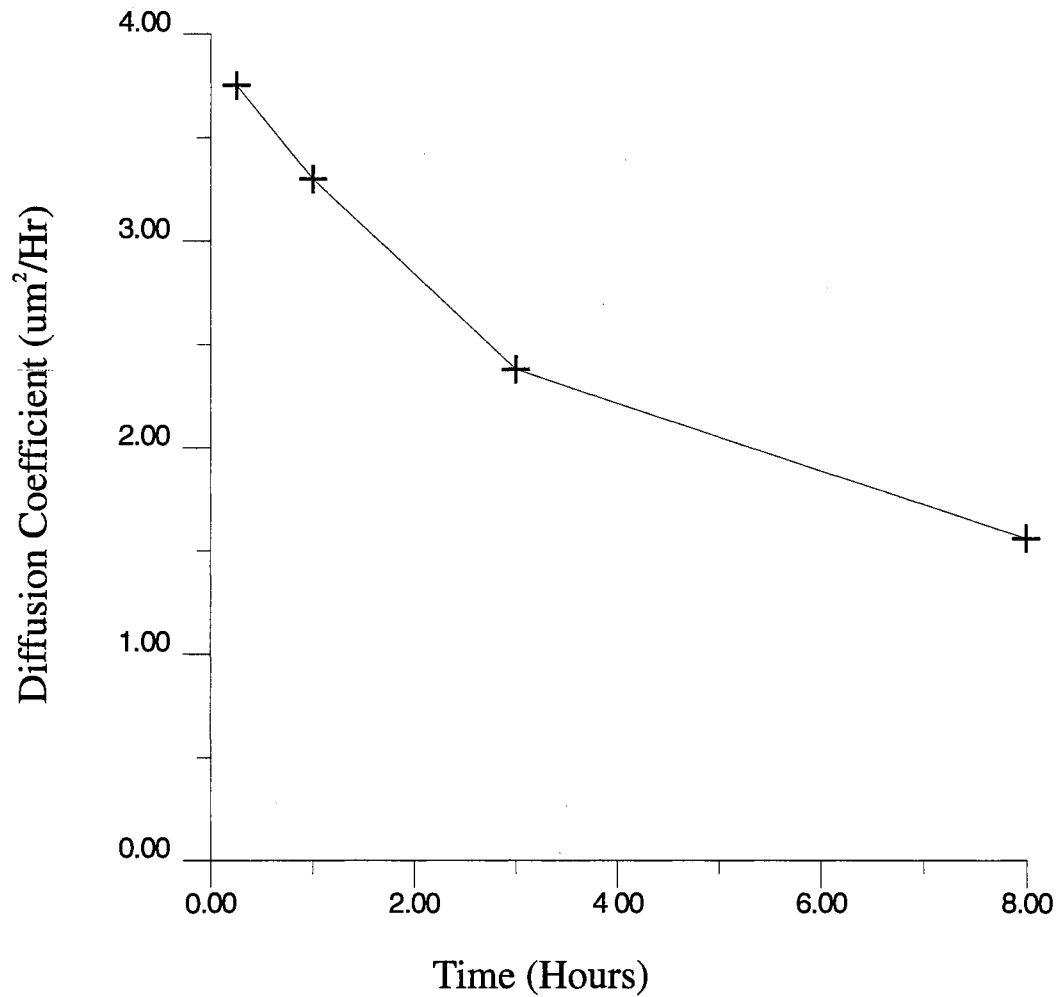


Figure 5.6. Diffusion coefficients for four different samples are plotted against the time in the salt bath.

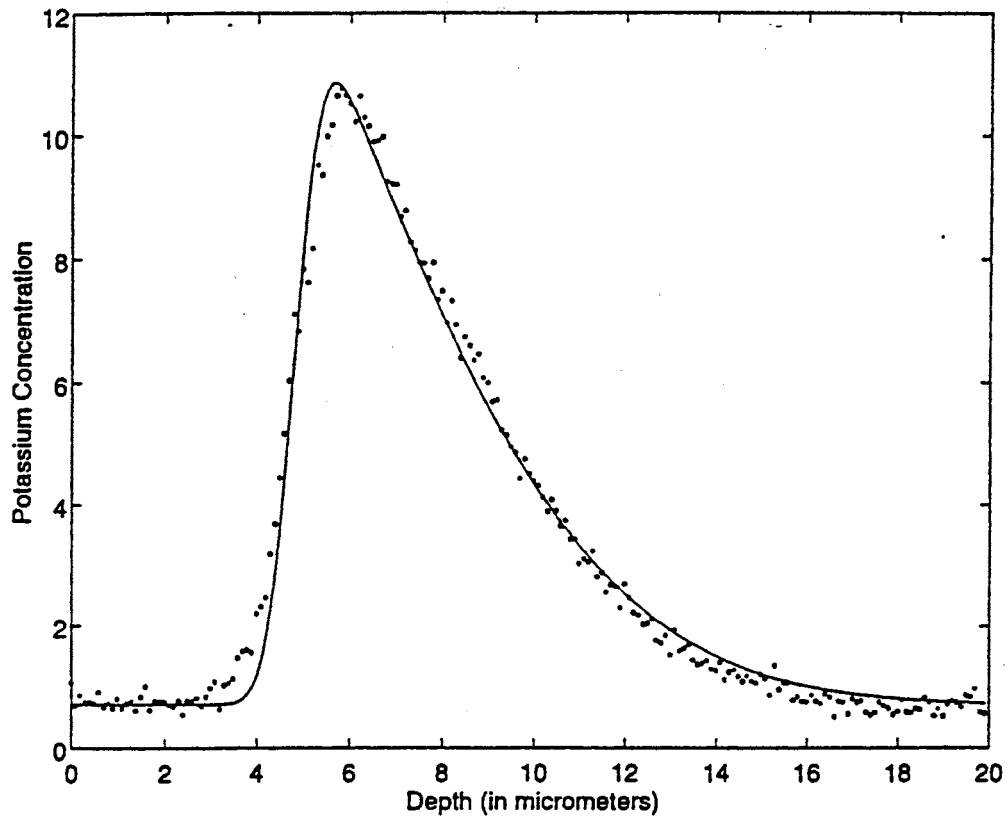


Figure 5.7. Curve fit of x-ray linescan and theoretical model for 8 hours of ion-exchange in potassium nitrate.

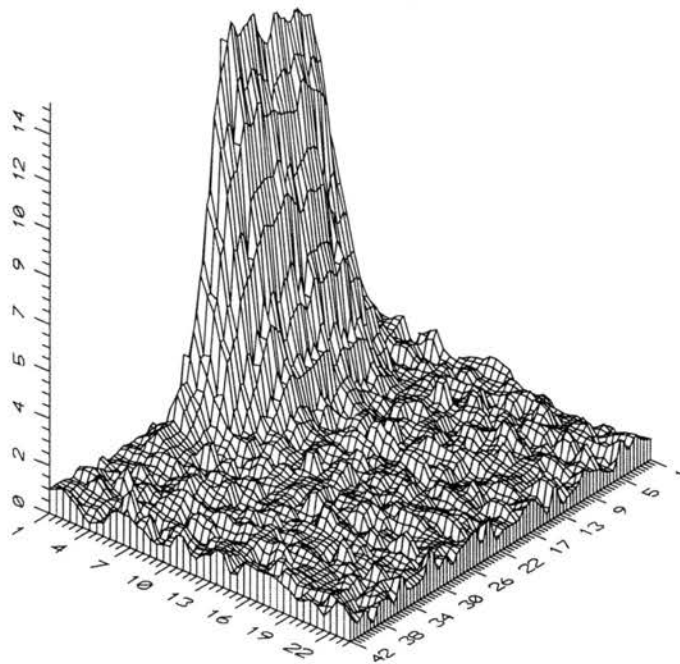


Figure 5.8. Two dimensional scan to obtain concentration profile using X-Ray analysis. This plot is for Corning 2947 ion-exchanged for 2.5 hours.

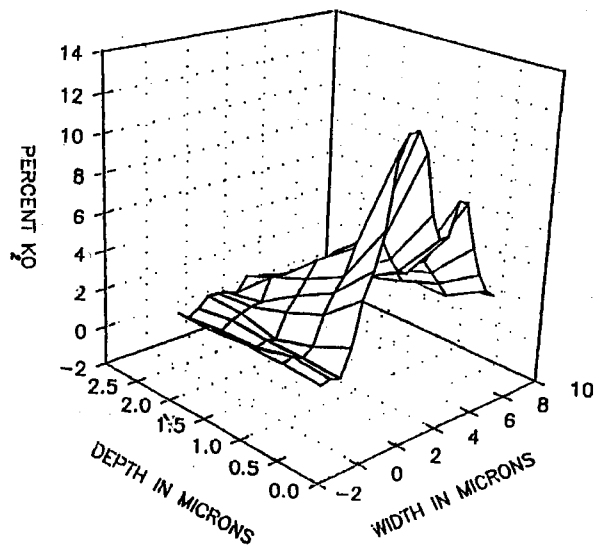


Figure 5.9. Two dimensional quantitative X-Ray scan for a channel waveguide. The profile displays a dip in the concentration indicating a hole in mask during ion-exchange.

This dip could not be easily detected or understood without a definitive picture such as this. The dip displays a hole in the mask that allows ion-exchange to occur beyond the boundaries of the mask. The profile is certainly affected by this.

Optical profile

The x-ray profile can be coupled with the optical profile of the waveguide for more complete information and can be observed using an optical scope. The optical profile for a fiber optical channel waveguide will display a circular pattern with the highest intensity at the center. A circular guided wave mode for ion-exchanged waveguides which have not been buried is not possible. Figure 5.10 demonstrates the optical profile for a nine micrometer wide mask. The profile is a narrow strip of light, which when compared to Figure 5.8 demonstrates how the shape of the potassium profile affects the far field diffraction pattern.

Modes in waveguides

The concentration profile of the waveguide and the optical profile are part of the characterization process for a waveguide. Determining the number of modes is also an important feature. This can be done most efficiently by endfire coupling into a planar waveguide and out-coupling through a prism. Each mode has a different exit angle clearly exposing the number of guided modes. A photograph of the output for this setup is shown in Figure 5.11.

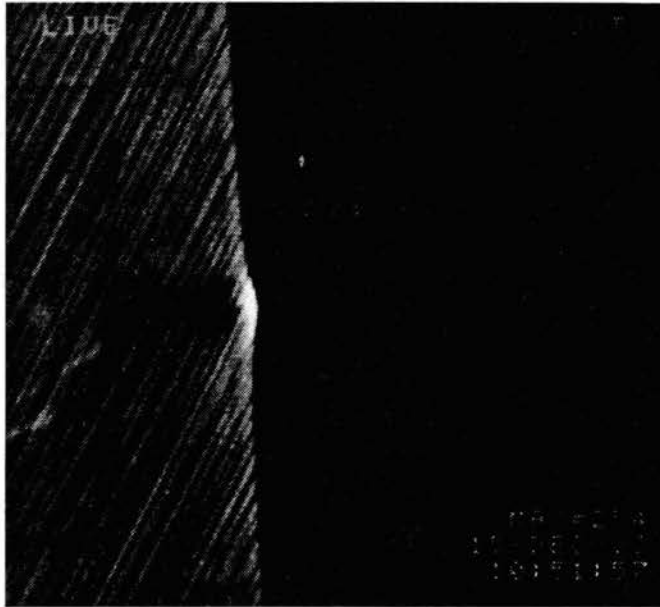


Figure 5.10. Far field diffraction using an optical scope. This is an ion-exchanged channel waveguide intensity profile.

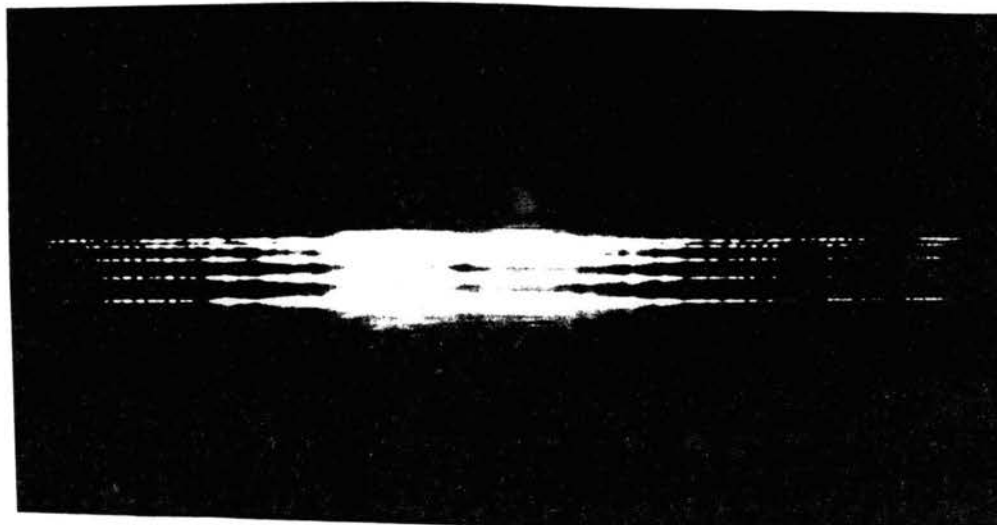
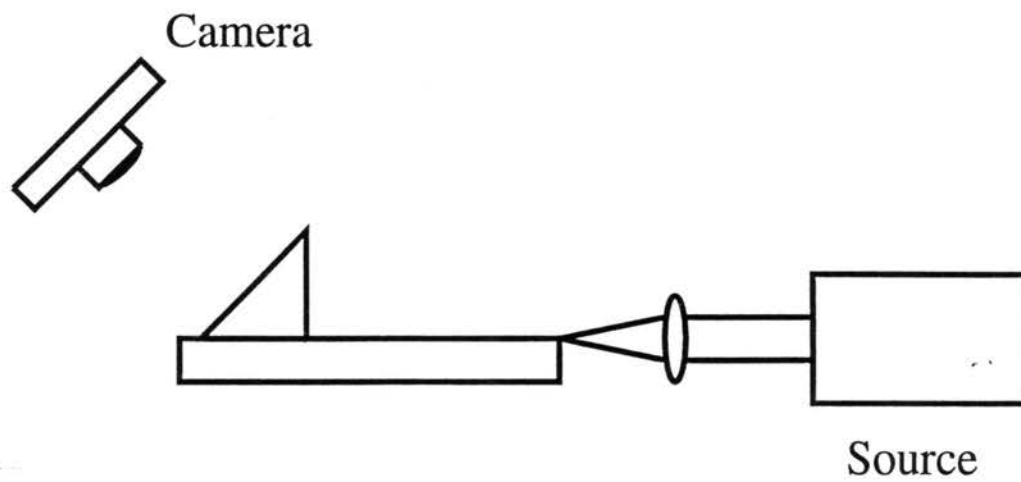


Figure 5.11. Modes from an ion-exchanged planar waveguide. Output was taken from a prism coupler.

Using this information coupled with the x-ray profile giving the diffusion depth and the information given in chapter II on modes in a planar waveguide, one can then estimate the times needed to create single and specific multi-mode waveguides. The effective depth is the criteria used for determining waveguide modes. The effective depth of the planar can then be determined as well using the three different techniques mentioned. This information can then be transferred over to channel waveguides to determine the number of modes in the y direction, the effective depth and the concentration profile.

Waveguide loss

Waveguide loss can be measured using several different methods. Each method has its advantages and disadvantages. The particular method chosen is to use a microscope objective and xyz translation stage. A detector is placed behind the objective with a metal casing completely surrounding both of these items to eliminate noise. This method is very similar to the bundle fiber method. The bundle fiber method is used to collect light and send this back to a detector. The microscope objective can be used to select a small point and then scan in a perpendicular motion across the guided light. The output is recorded from low to high and then back to low again. This produces a two-dimensional plot which represents one section of intensity. The microscope objective is then moved parallel to the guided light and the process is repeated. Figure 5.12 displays the experimental setup to measure waveguide loss.

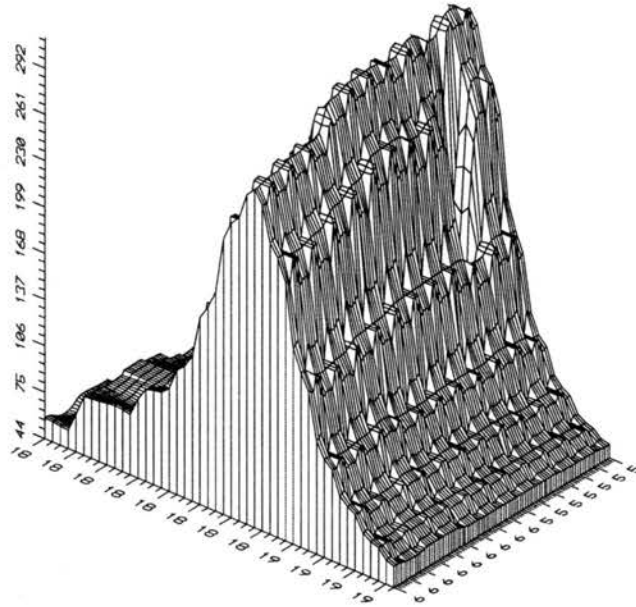
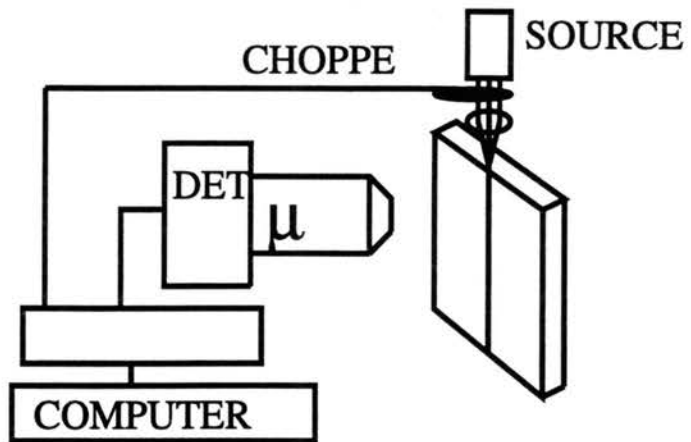


Figure 5.12. Waveguide loss setup and output for a Corning 2947 channel waveguide.

The lenses can be interchanged to adjust the spot size at the focal length. One of the advantages of this method over the fiber bundle is the focus in the z-direction. A maximum is obtained at a specified distance away from the glass thus promoting consistency. A second advantage is the variable lens provides control over the spot size. The resolution can be increased if needed for low-loss waveguides. This was set up and a loss measurement was taken on a channel waveguide fabricated in Corning 2947. The loss for this waveguide was 4.8 dB/cm. This was taken using a HeNe as a source (632.8 nm). It should be noted that only 1.1 mm length was needed to obtain loss measurements. The output is also shown in Figure 5.12.

Characterizing a material varies depending on the desired output. If a material has a rare earth doping in it is useful to have the above information plus the absorption spectrum, fluorescence lifetime of the material, the fluorescence spectrum and the gain. Techniques to accomplish this are discussed in the next chapter.

CHAPTER VI

NEODYMIUM WAVEGUIDE LASER

This chapter presents the fabrication and characterization of the neodymium-doped waveguide laser. Several different host materials were experimented with until a suitable material was found which would raise the refractive index after ion-exchange. Three of the glasses are silicate base glasses, LG-680, BK-7, S-3 and one is a phosphate base glass, APG-1. Two of the glasses, LG-680 and APG-1, have lithium as the loose bond or network modifier. The network modifier is the ion which is released from the glass during ion-exchange. BK-7 and S-3 have sodium as the network modifier. LG-680 and APG-1 are both available in the commercial market and are designed with a high gain cross section. BK-7 has been used to make a neodymium waveguide laser³⁶ providing a base for comparison with the other glasses. S-3 is not available as a commercial laser glass, however it was doped with 3% neodymium by weight. S-3 was chosen because it was designed specifically for ion-exchange. A waveguide laser was fabricated and tested using ion-exchange techniques described in chapter IV.

Glass characteristics

Initially one must determine whether an 'off-the-shelf' glass will ion-exchange. The glass must contain ions with loose bonds or network modifiers. The transformation temperature of the glass must be high enough to avoid a complete structural change in the glass when immersed in the salt bath. Potassium was used for as the exchange ion since

it produces a lower loss waveguide than silver. The melting point for KNO_3 is approximately $335\text{ }^\circ\text{C}$, depending on its purity. The transformation temperature of the glass must therefore be greater than $335\text{ }^\circ\text{C}$. Schott Glass Technologies has two different 'off-the-shelf' laser glasses which fit the above criteria: APG-1 and LG-680.

APG-1 is a phosphate base glass with 3% neodymium doped into a host containing both lithium and aluminum. The gain cross section for this glass as stated by Schott Glass is $3.5 \times 10^{20}\text{ cm}^2$. The transformation temperature is $450\text{ }^\circ\text{C}$. The LG-680 contains 3% neodymium doping in a silicate-based glass containing lithium, calcium and aluminum. The gain cross section for this glass as stated by Schott Glass is $2.9 \times 10^{20}\text{ cm}^2$. The transformation temperature is $468\text{ }^\circ\text{C}$. These glasses have proven to be good laser glasses because of the high gain cross section. They are known to be easily ion-exchanged since ion-exchange is commonly used by glass companies to strengthen the glass.

Ion-exchange

The APG-1 was ion-exchanged in potassium nitrate at $390\text{ }^\circ\text{C}$ for four hours. The glass displayed micro-cracking on random parts of the polished surface. This effect is shown in Figure 6.1. An x-ray line scan was taken as described in chapter IV. The line scan output should follow a typical diffusion profile. The first photograph in Figure 6.2 displays a shoulder where a smooth transition should appear. The profile indicates ion-exchange did take place, but it appears to degrade the surface. Since this glass is typically

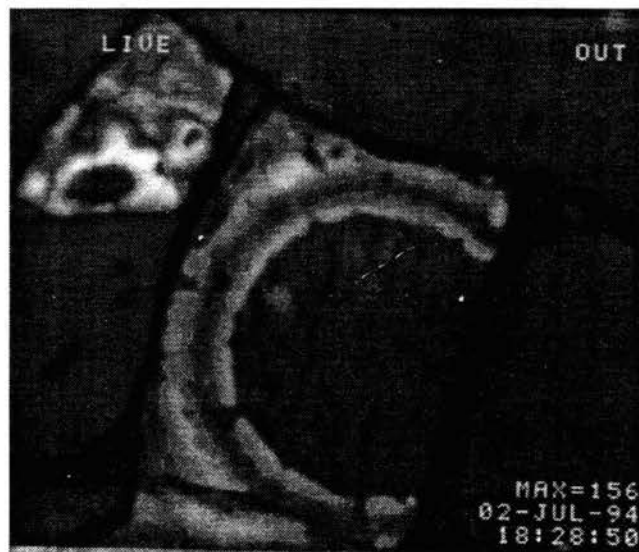


Figure 6.1. Photograph of APG-1 after 4 hour ion-exchange in potassium nitrate at 390 °C.

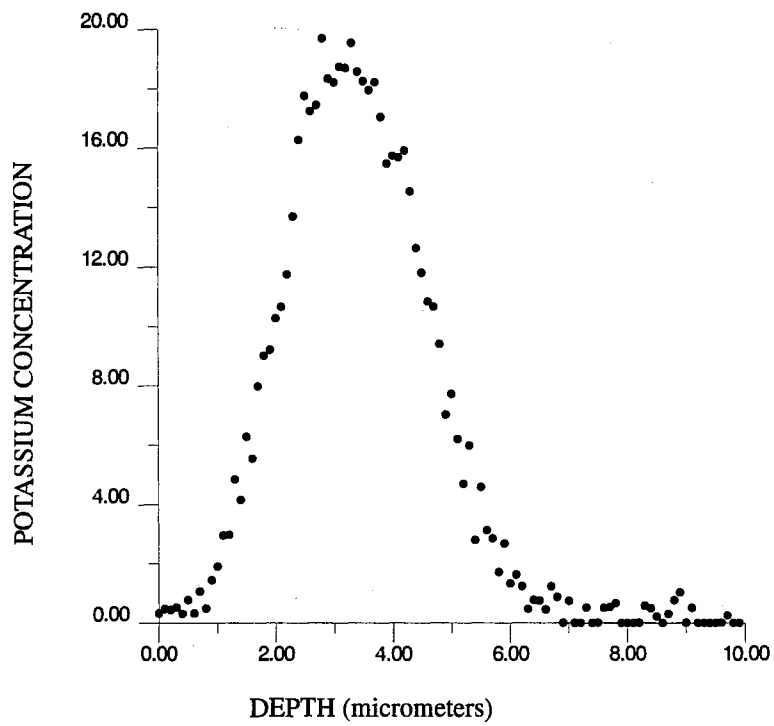
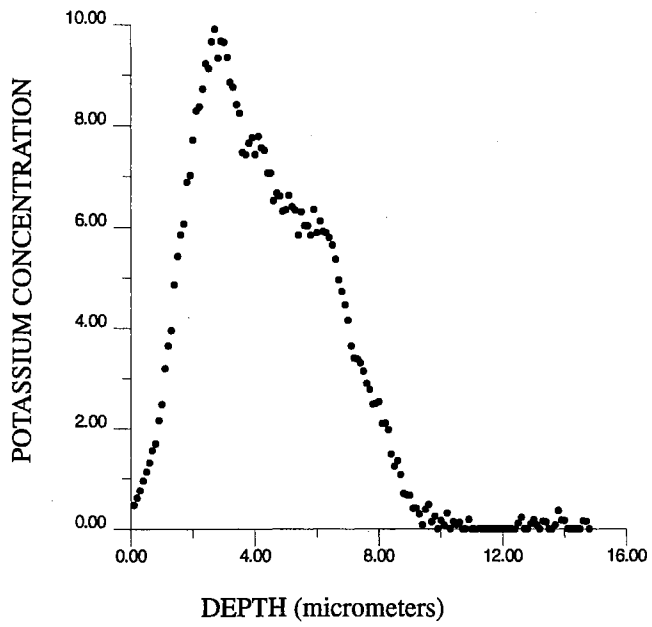


Figure 6.2. APG-1 ion-exchanged for four hours in potassium nitrate. The first plot was done at a temperature of 390 °C. The second plot was done at a temperature of 342 °C.

ion-exchanged as a strengthening tool, successful ion-exchange should be possible. The temperature was lowered closer to the melting point of potassium nitrate and ion-exchanged a second time. The outcome was a smooth surface with no micro-cracking. The x-ray line scan for this is shown in the second photograph of Figure 6.2. This figure displays a typical diffusion profile. An attempt to couple light into the ion-exchanged guide was unsuccessful.

The LG-680 was treated in a similar manner as the APG-1 with similar results. A thin film was apparent on the surface of the glass which when looked at closer displayed micro-cracking. A photograph of the surface is shown in Figure 6.3. The x-ray line scan for this is shown in plot of Figure 6.3. The profile did not appear unusual except that the depth of the diffusion was very shallow for a four hour exchange. The temperature was lowered to determine if the thin film would disappear. The LG-680 was ion-exchanged a second time at 342 °C. The surface was clear in spots, but did not appear completely smooth as did the APG-1. Since Schott Glass typically strengthens this glass successfully with sodium exchange, a third ion-exchange was done at a temperature of 320 °C in sodium nitrate for four hours. The surface was clear after the exchange. The ends were polished and an attempt to couple light into the waveguide via endfire coupling was not successful.

The next two glasses tried were BK-7 and S-3. These glasses are both silicate-base glasses which are commonly used for potassium ion-exchange. BK-7 is a common

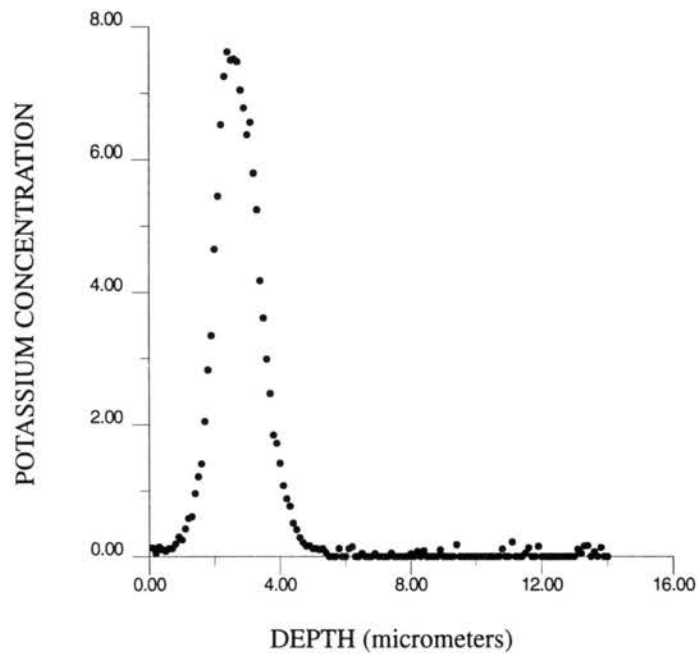
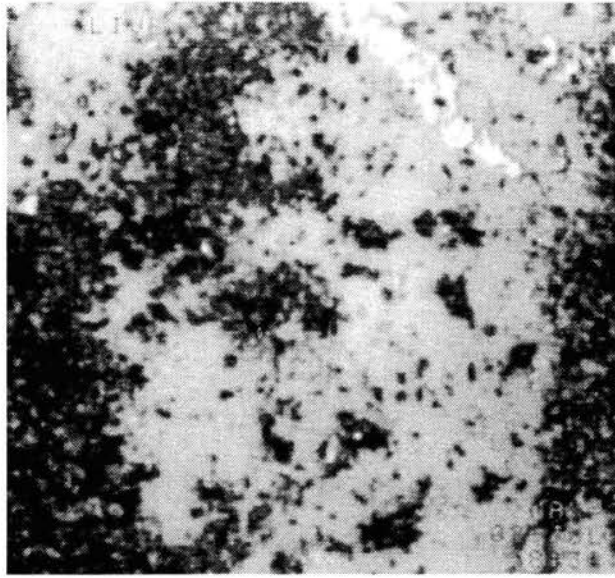


Figure 6.3. LG-680 ion-exchanged at 390 °C for four hours in potassium nitrate. The top photograph shows microcracking. The plot displays a normal diffusion profile, however it is very short.

glass used in making lenses and other bulk optical pieces because of its good optical properties. BK-7 has been doped with neodymium and ion-exchanged to make a waveguide laser.³⁶ S-3 is an ophthalmic glass developed by Schott Glass and designed specifically for ion-exchange. Glasses with a mixture of zinc and no mixture of calcium provide good ion-exchange qualities as noted by Stroud.⁴⁶ Neither of these glasses are commercial laser glasses since a laser glass is designed specifically to have a high gain cross section. A combination of good ion-exchange characteristics and high gain cross section would be the optimal glass to use for developing waveguide lasers. This work has not been completed. Studies of the ion-exchange properties of neodymium doped glass are still being conducted by NIST & Schott.¹⁰

BK-7 is a mixed-alkali glass containing barium and borosilicate. The transformation temperature of the BK-7 is 557 °C. This glass was doped by Schott Glass with 3% Nd. The gain cross section was determined by Stokowski⁴⁵ to be $1.3 \times 10^{20} \text{ cm}^2$ for 3% Nd doping. S-3 is a mixed Alkali glass with high concentrations of Zinc and Silicate. The Zinc in this glass enhances the ion-exchange capabilities⁴⁶. S-3 was doped by Schott Glass with 3% Nd. The transformation temperature of this glass is 532 °C. Since this glass has not previously been studied, the gain cross section is not known.

The neodymium doped BK-7 was ion-exchanged at 390 °C for four hours. The polished surface appeared to be unchanged after ion-exchange. The x-ray linescan is shown in the first plot of Figure 6.4. A least squares fit to determine the diffusion

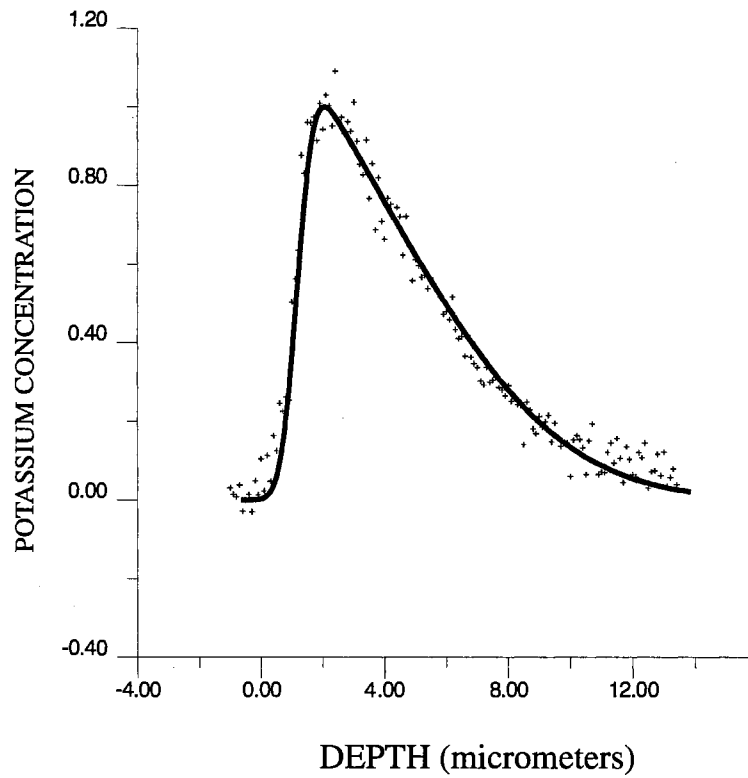
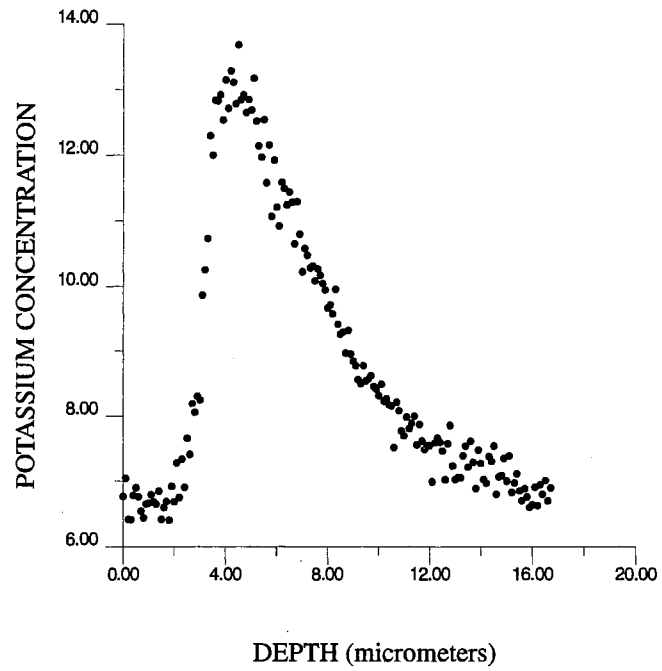


Figure 6.4. X-ray line scan for BK-7 after four hour ion-exchange in potassium nitrate. The second plot is a fit to determine the diffusion coefficient. For this particular glass the $D = 2.8 \text{ um}^2/\text{hr}$ and $M = 1.0$.

coefficient and ratio was done as explained in chapter V. The diffusion coefficient is $D = 2.8 \text{ um}^2/\text{hr}$ and the ratio is $M = 0.6$. The fit for this is shown in second plot of Figure 6.4. Light was successfully coupled into this guide via endfire coupling.

The neodymium doped S-3 was ion-exchanged at $390 \text{ }^\circ\text{C}$ for four hours. The results of this glass were similar to those of the BK-7 except the least squares fit showed a diffusion coefficient of $D = 8.9 \text{ um}^2/\text{hr}$ and a ratio of $M = 1.0$. The x-ray line scan and the least squares fit are shown in Figure 6.5. The diffusion coefficient is three to four times larger than the BK-7 or the Corning 2947. This can be attributed to the large amount of Zinc in the makeup of the glass. Stroud did a study on the effect of Zinc when ion-exchanging.⁴⁶ Light was successfully coupled into the waveguide via endfire coupling.

Backdiffusion

Both BK-7 and S-3 were successfully ion-exchanged to make surface waveguides. Surface waveguides produce less efficient waveguide lasers since scattering is much higher due to the surface imperfections. These two glasses were taken one step further and backdiffusion was attempted. After the initial ion-exchange of 4 hours in potassium nitrate, a second ion-exchange was done using sodium nitrate. This second ion-exchange removes the potassium ions on the surface of the glass thus leaving a buried waveguide. This proved to be true for the BK-7, but S-3 displayed severe micro-cracking over the entire polished surface. Figure 6.6 shows photographs of S-3 and BK-7 after four hours

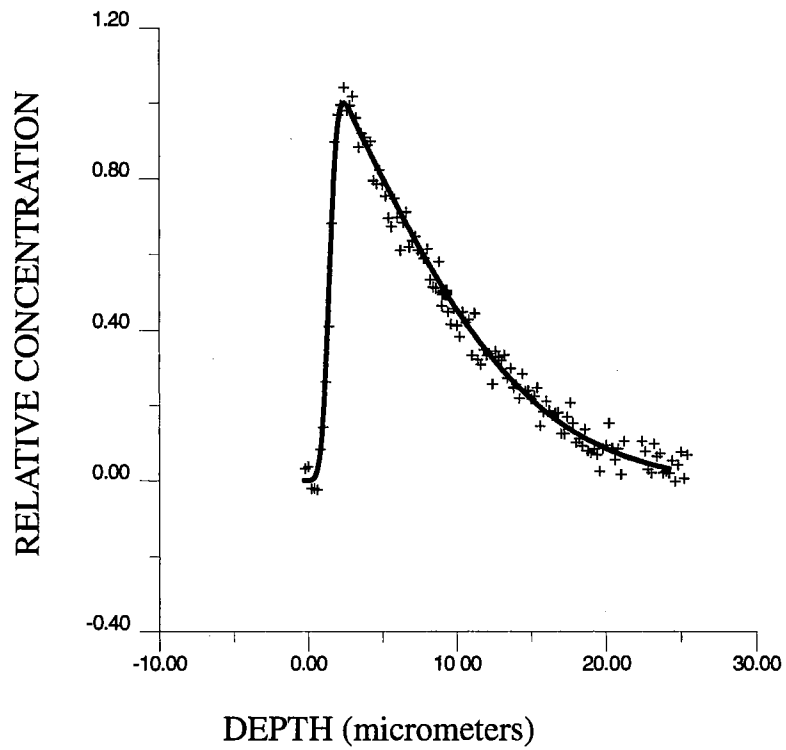
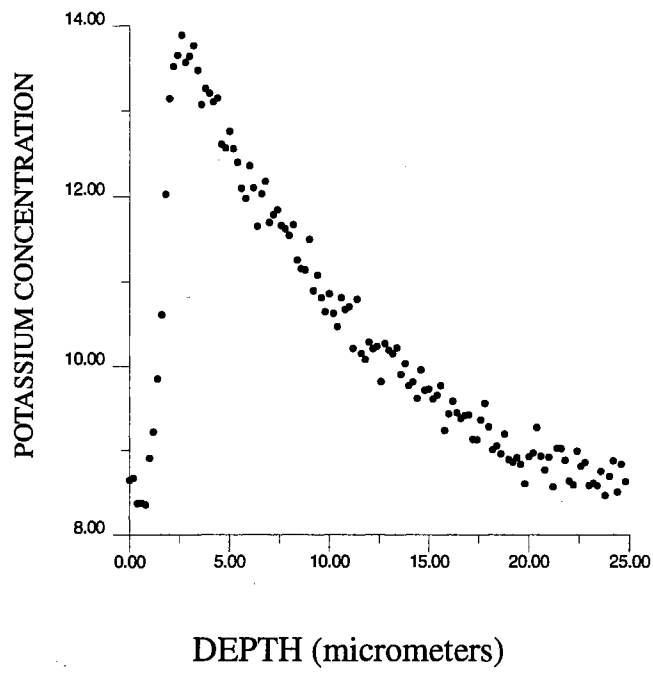


Figure 6.5. X-ray linescan and curve fit of S-3 for a four hour ion-exchange in potassium nitrate.

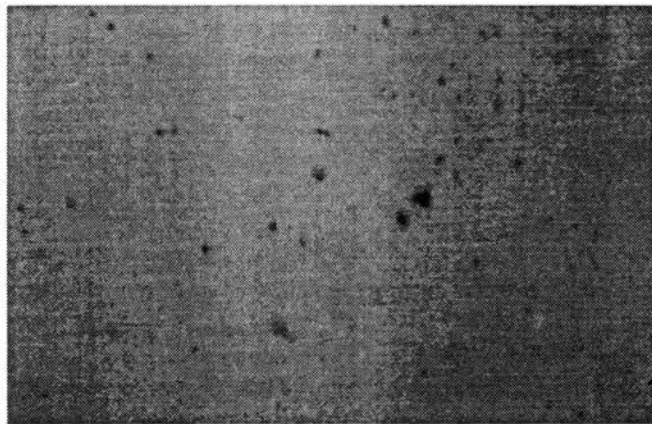
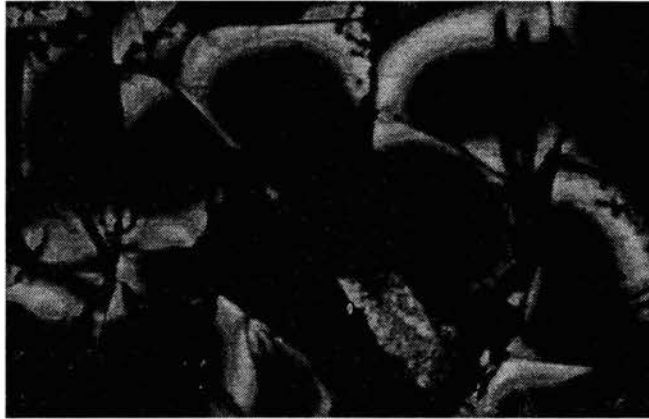


Figure 6.6. S-3 and BK-7 ion-exchanged in potassium nitrate for four hours, then ion-exchanged a second time in sodium nitrate for half an hour. The S-3 shows microcracking.

of ion-exchange in potassium nitrate and a half an hour second ion-exchange in sodium nitrate. Backdiffusion was attempted several times in S-3 with the same result each time. A possible solution which would need to be pursued for confirmation would be to mix a second nitrate solution with the sodium nitrate to slow down the exchange process. Adding potassium nitrate to the sodium nitrate would slow down the ion-exchange process and possibly stop the micro-cracking. This was suggested by Dave Sapak with Schott Glass. Sapak also suggested that a depletion of potassium probably occurred at the surface of the glass. This suggestion was confirmed by line scanning the backdiffused S-3. Figure 6.7 shows the depletion of potassium ions on the surface.

Laser characterization

The transmission spectrum, the fluorescence spectrum and the fluorescence lifetime were all measured for the neodymium doped S-3 using a bulk piece of glass. The transmission spectrum was obtained using a Cary 2400S spectrophotometer. This is shown in Figure 6.8. This spectra contains the obvious characteristics of strong absorption peaks at 580 nm and 805 nm as well as the minor absorption peaks which neodymium doped glasses possess.

The fluorescence spectrum of the glass can be obtained by pumping the glass with 805 nm and taking the output behind a monochromator. The setup for this experiment is shown in the first plot of Figure 6.9. A lock-in amplifier is used to overcome the small signals obtained from the fluorescence. The second plot in Figures 6.9 shows a plot

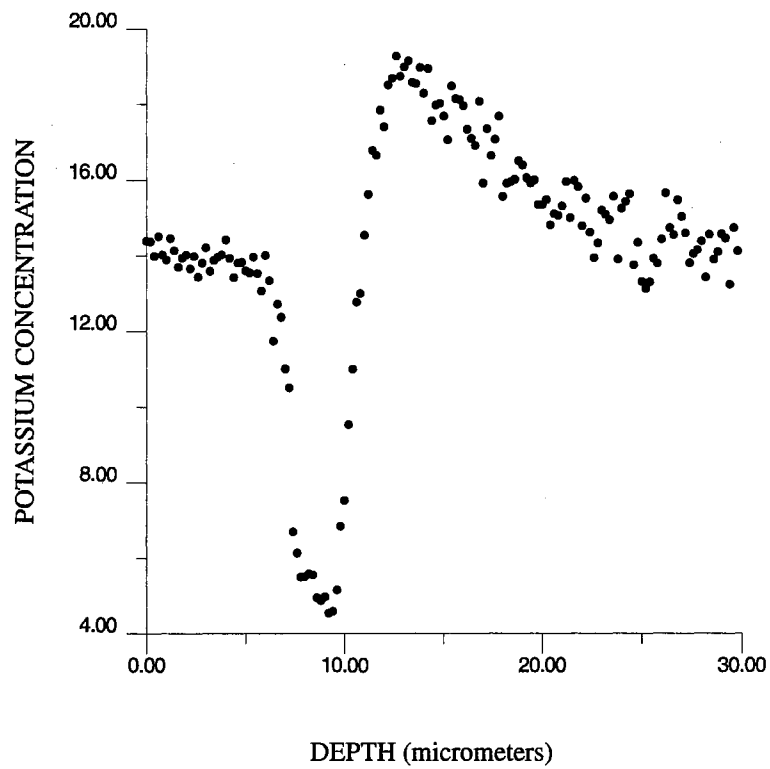


Figure 6.7. X-ray linescan of S-3 backdiffused, the potassium depletion is evident in the dip area.

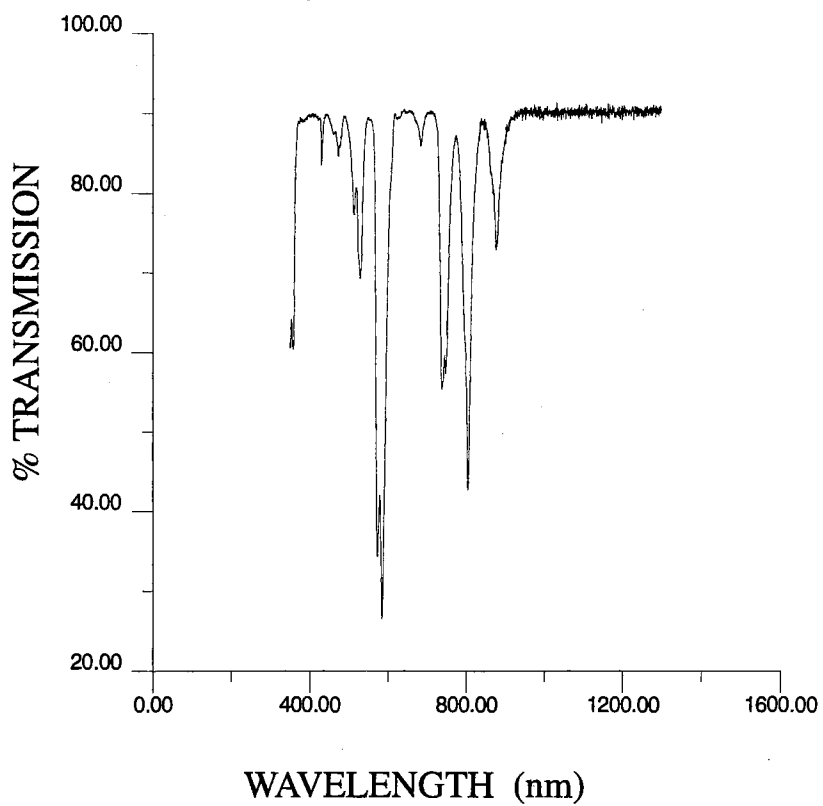


Figure 6.8. Transmission spectrum of 3% Nd doped S-3 glass. The absorption strong absorption peaks are at 580nm and 805nm..

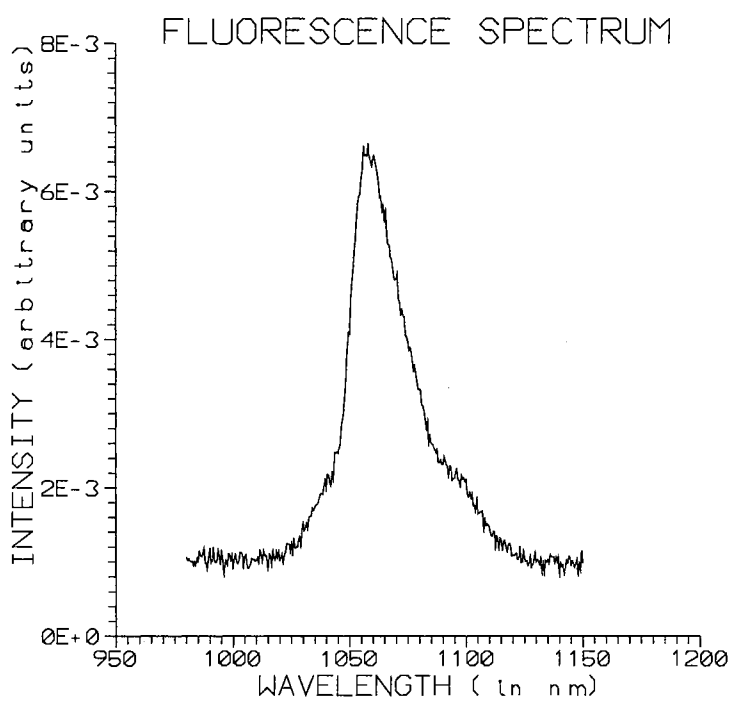
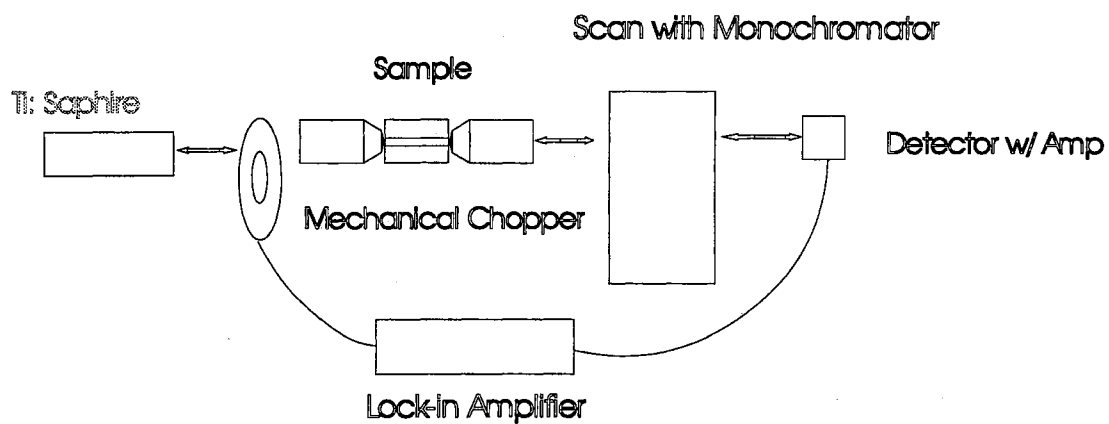


Figure 6.9. Setup and output for the spectrum of the fluorescence for Nd doped S-3.

displaying a spectrum covering 975 nm to 1050 nm with the peak centered around 1054 nm.

Fluorescence lifetime can be obtained from a gain medium by exciting the medium with a short pulse. The pulse must be several orders of magnitude shorter than the lifetime of the neodymium. The source for the short pulse is obtained from a pulsed nitrogen laser. This is not optimal with respect to absorption but it is adequate. The nitrogen laser lases at 337 nm with a pulse width of 600 ps. It is expected that the fluorescence lifetime of the Nd glass will be on the order of hundreds of microseconds. The setup for the fluorescence lifetime measurement is shown in the diagram of Figure 6.10 along with the output for this measurement. The resulting signal is an exponential decay. Taking the fluorescence lifetime to be the $1/e$ of the peak fluorescence signal yields a value of approximately 250 us.

Comparing the S-3 data with the other glasses shows no significant difference in the transmission spectrum or the fluorescence spectrum although the fluorescence lifetimes varied from glass to glass. The longest fluorescence lifetime resulted from the BK-7, and the shortest lifetime from the S-3. Table 6.1 displays the glass and lifetime that was measured.

Channel waveguide laser

Channel waveguides were made in the neodymium doped S-3 glass as discussed

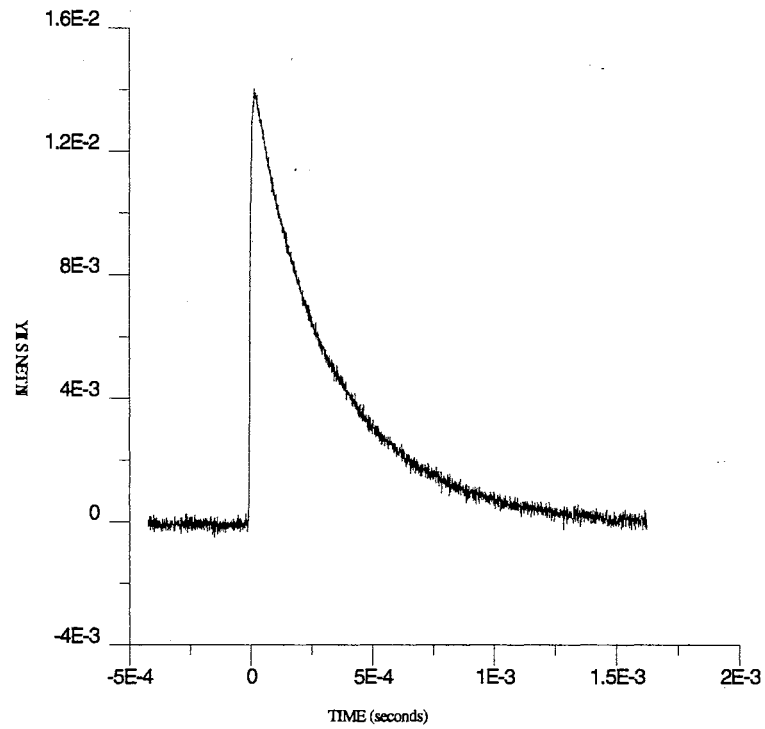
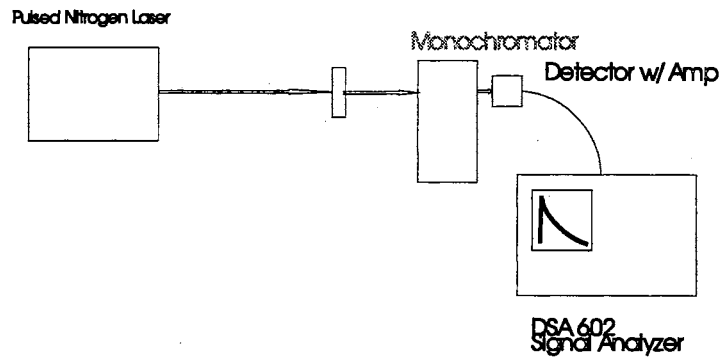


Figure 6.10. Experimental setup and output for fluorescence lifetime taken on Nd doped S-3.

GLASS TYPE	LIFETIME (in microseconds)
APG-1	360
LG-680	310
BK-7	405
S-3	280

Table 6.1. Fluorescence lifetime for each glass. This was done using a short pulsed laser and measuring the decay at $1/e$ from the peak.

in chapter IV. The length of the waveguides after polishing was approximately 1 cm. The width of the channels varied from a few microns to as much as 200 microns. Since the waveguide is on the surface of the glass and less than 25 microns deep, the edge of the glass must be perpendicular to the surface of the glass. A rounding effect takes place while polishing, so it is critical to protect the edge by pressing a second piece of glass against the surface (discussed in chapter IV) to avoid a lensing effect. These two effects can prohibit the neodymium doped channel waveguide from lasing. A third item to ensure a proper laser cavity, is the alignment of the channels with respect to each edge. A perpendicular alignment must be made between the channel and the edge of the glass. Each channel waveguide has an acceptance angle which must be considered when trying to reflect light back into the waveguide. If the angle is exceeded the neodymium doped channel waveguide will not lase. All three of these issues are taken care of during the polishing process. Proper sample mounting and holding for the polish is critical to ensure that the waveguide edge is perpendicular to the channel and rounding or large spacings are minimized.

To make the neodymium channel waveguide lase, mirrors must be placed on each end. The mirrors are made using dielectric coatings which have high transmission at 800 nm. One mirror has a near 100% reflector around 1060 nm. The other mirror has approximately a 95% reflector at 1060 nm. Cover slides were coated by Colorado Research Inc. and used as the mirrors. The mirrors were placed against the neodymium doped waveguide with index matching fluid. This is then pumped with the Ti:Sapphire

laser at 805 nm. The output is taken from the 95% reflecting mirror behind an RG 850 filter. The setup for this experiment is shown in diagram of Figure 6.11.

The mirrors were attached to the end of waveguide using index matching fluid. This left a small gap of fluid between the dielectric coatings and the end of the glass. Focusing the pump laser on the end of the waveguide would cause the fluid to burn when the pump power was increased thus ruining the mirror and the end of the waveguide. At lower powers, if the beam was focused on the gap instead of the waveguide this also burned the fluid. Caution had to be taken to insure both proper power and focusing of the pump beam. The laser was pumped and the output was measured with a power meter after the pump source was filtered out. The output power versus the input power for the waveguide laser was recorded. The plot of Figure 6.11 displays the typical input vs. output laser characteristic with the threshold at approximately 130 mW. It should be noted that this is the power from the pump laser and not the power coupled into the waveguide.

A successful Nd waveguide laser was made using S-3. Two improvements need to be made before this laser could be a commercial item. Burying the waveguide for lower loss, thus providing a more efficient laser. Coating the ends of the waveguide directly with dielectric coatings will eliminate both the gap and the oil in the gap. This will allow a higher power to be pumped into the waveguide without destroying the device as well as providing a stable, easy to implement laser source.

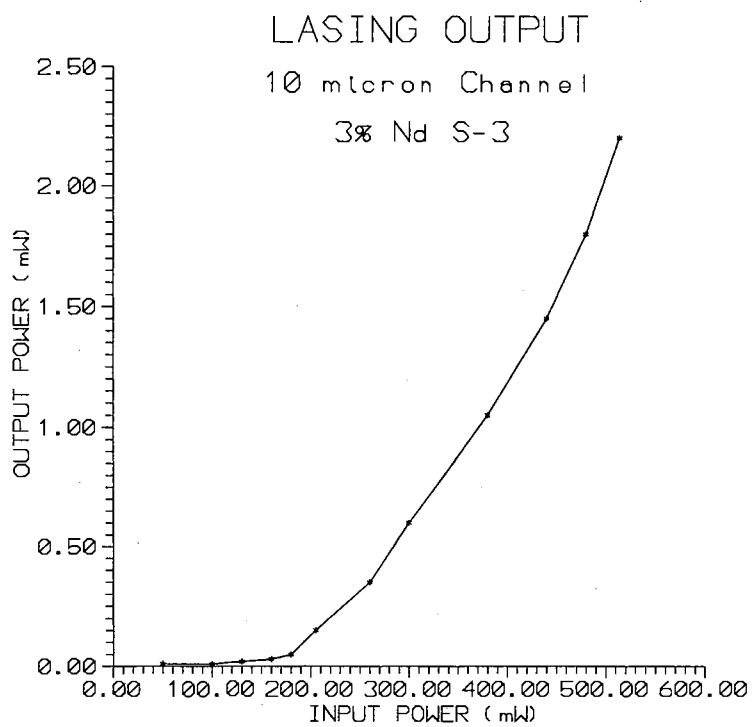
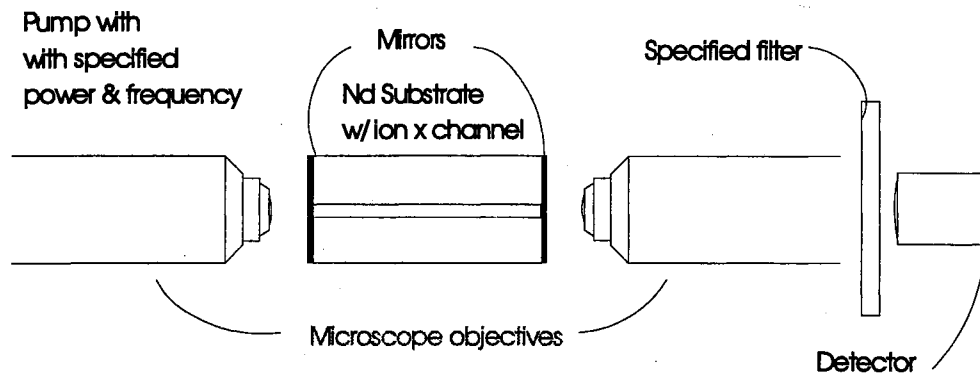


Figure 6.11. Nd waveguide laser setup and output power from a 9 micron channel.

CHAPTER VII

CONCLUSION

Summary

The theory of ion-exchanged planar waveguides was described with numerical models for comparison with theory. The diffusion equations were used to define the profile of ion-exchanged planar waveguides. This was compared with the experimental output obtained from the quantitative output of x-ray analysis. X-ray analysis was done by taking two pieces of glass and pressing them together until optical contact was obtained. This allowed the observation of the concentration profile without distortion due to the interaction volume. The interaction volume determined the spatial resolution of the x-ray scan. A second piece of glass pressed together with the original glass allowed for higher accuracy.

The accurate experimental data was then taken and compared with the theoretical model by using a least squares fitting routine. From this the diffusion coefficient and the ratio of the diffusion coefficient can be determined accurately. This technique also allows a direct observation of the concentration profile of a channel waveguide. A more complete characterization can be done by comparing these results with results obtained from optical techniques. This also aids in the development of profile shaping. Direct observation of the concentration profile provides direct feedback for the controlling process. The controlling process includes thermal ion-exchange, field assist ion-exchange

and backdiffusion. These tools allow more control over the profile, which leads to a circular profile compatible with fiber optic cables.

These techniques can also be used to develop integrated optical devices such as an integrated optical waveguide laser. This was demonstrated in neodymium doped glass. The same techniques were used to develop an integrated waveguide in the neodymium doped glass. Mirrors were placed on the ends of the waveguide with high reflectors set at 1.06 nm. This was pumped with 805 nm and lasing observed. The ion-exchange waveguides were made in two separate and suitable glasses after it was tried in four different glasses. All glasses ion-exchanged but only two were able to guide light. The subsequent study of the glass indicated that the ion-exchange process raised the refractive index in only two glasses.

Recommendations

The x-ray microprobe technique was used to directly observe the concentration profile in soda-lime glass after ion-exchange with potassium. The ion-exchange time was varied and the diffusion coefficient was found to change with the time. This was discovered because the x-ray technique provided information for shallow depth waveguides. For long periods of ion-exchange the diffusion coefficient appears to become constant, matching what has been published by several authors. There is no existing model or explanation concerning the changing diffusion coefficients for short ion-exchange times.

The S-3 glass is suitable for both ion-exchange and making waveguide lasers. The S-3 laser has not been completely characterized and compared with existing waveguide lasers made from other host materials, such as BK-7. Once the complete characterization of the waveguide laser has been completed, passively mode-locking the laser could be attempted.

REFERENCES

REFERENCES

1. Iraj Najafi and Chunmeng Wu, "Potassium Ion Exchanged glass Waveguide Directional Couplers at 0.6328 and 1.3 μm ," Applied Optics Vol. 28, No. 13, pp. 2459-2460 (1989).
2. Eiji Okuda, Ichiro Tanaka, and Tetsuya Yamasaki, "Planar Gradient-Index Glass Waveguide and its Applications to a 4-port Branched Circuit and Star Coupler," Applied Optics, Vol. 23, No. 11, pp. 1745-1748 (1984).
3. S. Honkanen, A. Tervonen, H. von Bagh, and M. Leppihalme, "Ion Exchange Process for Fabrication of Waveguide Couplers for Fiber Optic Sensor Applications," J. Appl. Phys. 61 pp. 52-56 (1987).
4. C. P. Hussell, R. V. Ramaswamy, R. Srivastava, and Janet L Jackel, "Adiabatic Invariance in GRIN Channel Waveguides and Its Use in 3-dB Cross Couplers," Applied Optics Vol. 29, No. 28, pp. 4105-4110 (1990).
5. H. C. Cheng and R. V. Ramaswamy, "Symmetrical Directional Coupler as a Wavelength Multiplexer-Demultiplexer: Theory and Experiment," IEEE J. Quantum Electronics, Vol. 27, No. 3 pp. 567-574 (1991).
6. R. Brinkmann, Electronic Letters, Vol 27, No. 5, pp. 42-44, (1994).
7. H. Suche, Electronic Letters, Vol 29, No. 12, pp. 1111-1113, (1993).
8. Eugene D. Jungbluth, "Optical waveguides advance to meet fiberoptic demands", Laser Focus World, pp 99-104, April 1994.
9. Martin McCourt, "Commercial glass waveguide devices", Critical Reviews of Optical Science and Technology, Vol CR53, pp 200-208, (1994).
10. Kevin J. Malone, "Integrated-Optical Devices in Rare-Earth Doped Glass", Critical Review of Optical Science and Technology, Vol CR53, pp 132-158, (1994).
11. T. Izawa, and H. Nakagome, "Silver Ion-Exchanged Glass Waveguides," Applied Physics Letters, Vol. 21, pp. 584-586

(1972).

12. S. Honkanen and A. Tervonen, "Experimental Analysis of Ag⁺-Na⁺ Exchange In glass With Ag Film Ion Sources for Planar Optical Waveguide Fabrication," J. Appl. Phys. 63, 3, pp. 634-639 (1988).

13. S.I. Najafi, R. Srivastava, and R. V. Ramaswamy, "Wavelength-dependent Propagation Characteristics of Ag⁺-Na⁺ Exchange Planar glass Waveguides," Applied Optics. Vol. 29, No. 8, pp. 1840-1843 (1990).

14. Hsing C. Cheng and Ramu V. Ramaswamy, "Simulation of Tapered Transitions in Ion-Exchanged Channel Waveguides," Applied Optics. Vol. 29, No. 8, pp. 1150-1156 (1990).

15. B. Pantchev and Z. Nikolov, "Method of Refractive Index Profile Reconstruction from Effective Index of Planar Optical Monomode Waveguides: Application to Potassium Ion - Exchanged Waveguides," IEEE J. Quantum Electron. Vol. 29, No 1, pp. 154-160 (1993).

16. Amalia N. Miliou, Ramakant Srivastava, and Ramu V. Ramaswamy, "Modeling of the Index Change in K⁺ -Na⁺ Ion-Exchange glass," Applied Optics. Vol. 30, No. 6, pp.674-679 (1991).

17. L Zhou, J. Laybourn, V. Magill, and M. De La Rue, "Completely Buried Planar Waveguides Fabricated in glass using a Two-Step Purely Thermal K⁺ and Na⁺ Ion-Exchange," IEEE Proceedings-J, Vol. 139, No. 3, pp. 223-227 (1992).

18. S. Iraj Nafafi, Wei-Jian Wang, John F. Currie, Richard Leonelli and John L. Brebner, "Fabrication and Characterization of Neodymium-Doped glass Waveguides," IEEE , pp. 109 (1989).

19. Joseph E. Gortych and Dennis G. Hall, "Fabrication of Planar Optical Waveguides by K⁺ -Ion Exchange in BK7 and Pyrex Glass," IEEE J. Quantum Electronics. Vol QE-22, No. 6, pp. 892-895 (1986).

20. S. Iraj Najafi, "Introduction to Glass Integrated Optics," PP. 97 (1992).

21. R. V. Ramaswamy and R. Srivastava, "Ion-Exchanged Glass Waveguides: A Review," IEEE J. Lightwave Technology, Vol. 6, No.7, pp. 984-1001 (1988).

22. S. Iraj Najafi, Paul Gl Suchoski. Jr., and Ramu V. Ramaswamy. "Silver Film-Diffused Glass Waveguides: Diffusion Process and Optical Properties," IEEE J. Quantum Electronics.

Vol. QE-22, No. 12, pp. 2213-2217 (1986).

23. Ramu V. Ramaswamy and S. Iraj Najafi "Planar, Buried, Ion-Exchanged Glass Waveguides: Diffusion Characteristics," IEEE J. Quantum Electronics. Vol. QE-22, No.6, pp.883-891 (1986).

24. T. G. Giallorenzi, E. J. West, R. Kirk, R. Gunther, and R.A. Andrews, "Optical Waveguides Formed by Thermal Migration of Ions in Glass," Applied Optics, Vol. 12, No.6, pp. 1240-1245 (1973).

25. A. Miliou, H.C. Zhenguang, Ramakant Srivastava, and Ramu V. Ramaswamy, "Fiber-Compatible K⁺ -Na⁺ Ion-Exchanged Channel Waveguides: Fabrication and Characterization," IEEE J. Quantum Electronics, Vol. 25, No. 8, pp. 1889-1896 (1989).

26. C. De Bernardi, R. De Franceschi, C. Malvicino, S. Morasco, L Moro, M. Morra, A. Carnera, "Effects of Potassium Concentration and Induced Stress on the Refractive index Profile in K⁺ -Na⁺ Ion Exchanged glass Waveguides," CSELT Technical Reports, Vol. 17, No. 1, pp. 61-67 (1989).

27. R.G. Hunsperger, "Integrated Optics," University of Delaware, (1978).

28. M. Haruna, Y. Segawa and H. Nishihara, "Nondestructive and Simple Method of Optical-Waveguide Loss Measurement with Optimization of End-fire Coupling," Electronics Letters Vol. 28 No. 17, pp. 1612-1613 (1992).

29. R. K. Hickernell, D. R. Larson, R. J. Phelan Jr., and L. E. Larson, "Waveguide Loss Measurement using Photothermal Deflection," Applied Optics Vol. 27, No. 13, pp. 2636-2638 (1988).

30. Y. Okamura, A. Miki, and S. Yamamoto, "Observation of Wave Propagation in Integrated Optical Circuits," Applied Optics, Vol 25, No. 19, pp. 3405-3408 (1986).

31. S. I. Najafi, "Introduction to Glass Optics," pp. 124 (1992).

32. H. P. Weber, F. A. Dunn and W. N. Leibolt, "Loss Measurements in Thin Film Optical Waveguides," Applied Optics, Vol. 12, No. 4, pp. 755-757 (1973).

33. R. G. Walker, "Simple and Accurate Loss Measurement Technique for Semiconductor Optical Waveguides," Electron Letters, Vol. 21, No. 13, pp. 581-583 (1985).

34. N. A. Sanford, K. J. Malone, and D. R. Larson, "Integrated- Optic Laser Fabricated by Field-Assisted Ion Exchange in Neodymium-doped Soda-Lime-Silicate Glass." Optics Letters, Vol.15, No. 7, pp. 366-368 (1990).
35. H. Aoki, O. Maruyama, and Y. Asahar, "Glass Waveguide Laser,"
IEEE Photonics Technology Letters, Vol.2, No. 7, pp. 459-460 (1990).
36. E. K. Mwarania, L. Reekie, J. Wang, and J. S. Wilkinson, "Low-Threshold Monomode Ion-Exchanged Waveguide Lasers in Neodymium-Doped BK-7 Glass," Electronics Letters, No. 16, pp. 1317 (1990).
37. R. J. Gordon, and P. E. Jessop, "Optical Waveguide Laser using an rf sputtered Nd:Glass Film," Applied Optics, Vol.30, No. 3, pp. 276-278 (1991).
38. T. Tamir, "Intergrated optoelectronics",
39. Richard L. Liboff, "Introductory Quantum Mechanics", pp 241-252, (1992).
40. J. Albert, and G. L. Yip, "Refractive-index Profiles of Planar Waveguides Made by Ion-Exchange in Glass," Applied Optics, Vol. 24, No. 22, pp. 3692-3693 (1985).
41. R. V. Ramaswamy, H. C. Cawing and R. Srivastava, "Process Optimization of Buried Ag⁺ -Na⁺ Ion-Exchanged Waveguides: Theory and Experiment," Applied Optics, Vol. 27, No.9, pp. 1814-1819 (1988).
42. P. G. Noutsios and G. L. Yip, "Characterization and modeling of Planar Surface and Buried Glass Waveguides made by Field-Assisted K⁺ Ion Exchange," Applied Optics, Vol. 31, No. 25, pp. 5283-5291 (1992).
43. T. Poszner, G. Schreiter, and R. Muller, "Strip Waveguides With Matched Refractive Index Profiles Fabricated by Ion-Exchange in Glass," J. Applied Physics, 70 (4) pp. 1966-1974 (1991).
44. S. Iraj Najafi, "Introduction to Glass Integrated Optics", pp. 3-12, (1992).
45. Stokowski, Glass Technology Vol 27, No 2, May 1987.
46. J.S. Stroud, "The strengthening of some commercial ophthalmic and filter glasses by ion-exchange", Glass

Technology, Vol 29, No 3, pp 108-112, June 1988.

47. J. Richardson, Journal of Chemistry and Physics, Vol 34, 1979.

APPENDIX A2.1

Fortran program to estimate the number of modes in a given waveguide

```

If ((nf**2)*a)-(ns**2) .LT. 0.0) goto 15
c = sqrt((nf**2 * a) - nc**2)
phic = atan(c/(nf*b))

s = sqrt((nf**2 * a) - ns**2)
phis = atan(s/(nf*b))

v = (k*nf*b*ht(j) - phis - phic)/pi
mode(i) = int(v) + 1
angle=180.*zz/3.1415926
If (mode(i).NE. mode(i-1)) then
  If (mode(i) .EQ. 0) goto 422
*   print*, 'mode', int(v), ' at angle', angle
  write(j,210)ht(j)*scale,nf*sin(zz)
  End if
15  zz = zz + x
  goto 5

422  d1 = k*nf*b*h
     eff=nf*sin(zz)
210  format(3x,E12.4,3x,F12.4)
20   Continue

     close(1)
     close(2)
     close(3)
     close(4)
     close(5)
     close(6)
     close(7)
     close(8)
     close(9)
     close(10)
End

```

```

Real nf,nc,ns,h,y,pi,nd,k,uplimit,lolimit,count,N
Dimension mode(0:10000)
Dimension ht(1:10)
open(unit=1,file='num1.dat')
open(unit=2,file='num2.dat')
open(unit=3,file='num3.dat')
open(unit=4,file='num4.dat')
open(unit=5,file='num5.dat')
open(unit=6,file='num6.dat')
open(unit=7,file='num7.dat')
open(unit=8,file='num8.dat')
open(unit=9,file='num9.dat')
open(unit=10,file='num10.dat')

Do 3 i = 0,10000
    mode(i) = 0
3 Continue

    Num = 1000
*   Print*,'How thick is the film?'
*   Write(*,*)'The number you enter will be multiplie
*   Read(*,*)h1
    h1=4.0
    scale = 1e+6
    h = h1*1e-6
    maxht=10
*   Write(*,*)'What is the index of refraction of the
*   Read(*,*)nf
    nf = 1.55

*   Print*,'The cover is usually air.'
*   Write(*,*)'What is the index of refraction of the
*   Read(*,*)nc
    nc = 1.0
*   Write(*,*)'What is the index of refraction of the
*   Read(*,*)ns
    ns = 1.46
    i = 0
    Do 20 j = 1,maxht
    v = 1.
    y = .6328E-6
    pi = 3.14159
    nd = nc/nf
    k = 2*pi/y
    zz = asin(nd)
    x = (pi/2-nd)/Num
    zx = pi/2
    ht(j) = j*h/Float(maxht)
5   If ( v .LT. 0.0) goto 422
        i = i + 1
        a = sin(zz)**2
        b = cos(zz)
        N = nf*sin(zz)

```

APPENDIX A3.1

Explanation of finite difference method used

There are several different methods which can be considered and each has its advantage. I chose the same method Ari Tervonon (author of the glass waveguide section) which is the Dufort-Frankel method. This method does however require an initial set of values which can be obtained from the Euler method. The Dufort-Frankel finite-difference form is as follows:

$$\frac{C(i, n+1) - C(i, n-1)}{2\Delta t} = D \frac{C(i, n+1) - [C(i, n+1) + C(i, n-1)] + C(i-1, n)}{[C(i, n) (M-1) + 1] h^2} - \frac{MJ_o [C(i+1, n) - C(i-1, n)]}{[C(i, n) (M-1) + 1]^2 2h}$$

Initially we are working with just the thermal ion exchange without the electric field assist. The above equations are still valid, however the electric flux J_o which is proportional to the electric current density is set to zero. Therefore the last term in the equation will go to zero.

The desired unknown to solve is $C(i, n+1)$, and as can be seen from above this variable is on both sides of the equation therefore $C(i, n+1)$ must first be solved for algebraically. When this is done the following results:

$$C(i, n+1) = \frac{C(i, n-1) [C(i, n) (M-1) + 1] + k [C(i+1, n) - C(i, n-1) + C(i-1, n)]}{C(i, n) (M-1) + 1 + k} - \frac{k [[C(i+1, n) - C(i-1, n)]^2 (M-1)] [C(i, n) (M-1) + 1]}{4 [C(i, n) (M-1) + 1 + k] [C(i, n) (M-1) + 1]^2}$$

where $k = 2\Delta t D / h^2$. Notice the nonlinear term can be taken out of this simply by setting M

= 1. To obtain the initial values for starting this method there are directional terms involved therefore a very simple Euler form is used for one iteration. This method allows larger Δt 's to be used and still obtain a valid solution. To confirm whether or not this method is converging, several different step values for both Δt and h were used. In the above difference equation i is space and referenced to h and n is time referenced to Δt . The figure is for varying step sizes in the t direction. The standard which convergence is measure is taken from $\Delta t = .001$ seconds. At $\Delta t = 1$ second no solution was obtained.

This does truly converge and requires a step size in the t direction of about .002 seconds. A fortran program was written which took the data from each run and subtracted each run from the standard of $\Delta t = .001$ sec. The maximum was then found and noted. Four different step sizes were compared and the following is a summary of those results:

$\Delta t_1 = 0.1$ sec	Max diff = .169
$\Delta t_2 = 0.02$ sec	Max diff = .0251
$\Delta t_3 = 0.01$ sec	Max diff = .0116
$\Delta t_4 = 0.002$ sec	Max diff = .0013
$\Delta t_5 = 0.001$ sec	Each of the above compared to the values obtained here.

The following was used to determine the Max diff:

$$Maxdiff = \sqrt{f(\Delta t_5)^2 - f(\Delta t_1)^2}$$

convergence for different step sizes h . In this direction it is vary stable with little variation due to the large step size. However if the step size is too large then there will not be enough data to accurately determine what is going on in the diffusion process.

There is little variation between the large step size and the smaller step size. This data was run through the same program as above to determine the maximum difference between a standard value and the other step sizes.

$h = 0.5 \text{ um}$ Max diff = .014

$h = 0.25 \text{ um}$ Max diff = .003

$h = 0.1 \text{ um}$ Max diff = .0011

$h = 0.05 \text{ um}$ Max diff = .00097

$h = 0.02 \text{ um}$ Each of the above compared to the values obtained here.

These are maximum values which indicates the worst case. There worst case usually occurred in the middle of the curved part of the plot.

A second question which would be good to answer is the validity of the final solution. As can be seen from the above all of the plots appear to exponential. This is the solution to the linear diffusion equation. The exact solution is the complimentary error function and can be determined analytically

from the above equation. The nonlinear terms was taken out to obtain an analytical solution by simply setting $M = 1$. The solution for this is as follows:

$$C=0.5 \left[\operatorname{erfc}\left(\frac{x-J_0t}{2\sqrt{Dt}}\right) + \exp\left(\frac{J_0x}{D}\right) \operatorname{erfc}\left(\frac{x+J_0t}{2\sqrt{Dt}}\right) \right]$$

This can be plugged into a canned math package and plotted. The package I used to do this was **Mathematica**. This package has the complementary error function built in and allows easy access to plots also. To compare to the solutions which were obtained by my program set $J_0 = 0$. The plot is therefore the analytical solution for thermal diffusion only.

As can be seen from the table above at time $t = 100$ sec there is a very good match between the numerical solution and the analytical solution. From this we can conclude that the linear part of the numerical model is accurate. To determine whether or not the nonlinear part of the model works can only be done at this point by making sure the derivation of the solution is correct. After grinding through the math my results did match Ari Tervonen the author of the section on "Theoretical Analysis of Ion-Exchanged Glass Waveguides" in the Integrated Optics book. He also produced a couple of plots in his book, however his numbers did not match the analytical or my numerical output. Therefore I concluded the numbers he said he used in his program he did not use. However, the plots were consistent in shape with each other at $M = 1.0$ and $M = 0.1$. This last plot is for a constant time of 100 sec while all other variables are the same as above, except for the ratio of self-diffusion constant which I varied from $M = .9$ to $M = .1$ in steps of .2. The plots mentioned are shown in Figures 3.2 and 3.3 in Chapter III.

APPENDIX A3.2

Fortran program to provide a least squares fit for data

```

Integer ix,nt
Real*8 k,M,nlnr,k1,nlnr2
Real*8 elsq, minelsq, Delsq, Welsq, Selsq
Real*8 cnp(0:1001), cn(0:1001)
Common cnf(0:1001),x(0:1001),psum(0:1001)
Common x2(0:1001),shift

Open(unit=1,file='jun20e3.dat')

* total time = nt*delt (hours)!!!!!!!!!!!!!!!!!!!!!!!!!!!!!!
  nt = 40000
  delt = .0001
* total distance = ix * h (microns)!!!!!!!!!!!!!!!!!!!!!!!!!!!!!!
  ix = 560
  h = .05

* Non-linear term, M=1 implies linear!!!!!!!!!!!!!!!!!!!!!!!!!!!!!!
  M =1
* This is the width of the Gaussian shape!!!!!!!!!!!!!!!!!!!!!!!!!!!!!!
  wid = 12

* Diffusion constant!!!!!!!!!!!!!!!!!!!!!!!!!!!!!!!!!!!!!!!!!!!!!!
  D = 8.9

  k1 = delt*D/(h**2)
  k = 2*delt*D/(h**2)
  nm = 1

* number of experimental points!!!!!!!!!!!!!!!!!!!!!!!!!!!!!!!!!!!!!!
  npnts = 124

Do 30 i = 0,ix
  cnp(i) = 0.0
  cn(i) = 0.0
  cnf(i) = 0.0
30 Continue

  cnp(0) = 1.0
  cn(0) = 1.0
  cnf(0) = 1.0

Do 60 i = 1,ix
  cnf(i)=cn(i)+( cn(i+1)-2*cn(i)+cn(i-1) )*k1
  cn(i) = cnf(i)
60 Continue

Do 70 n = 1,nt
  Do 80 i = 1,ix
    nlnr = cn(i)*(M-1.0) + 1.0

```

```

Subroutine filtf(h,mpts,wid)
Common cnf(0:1001), x(0:1001), psum(0:1001)
real*8 f(0:1001)
real gg(0:1001)
open(unit=3,file='vol6.dat')

* This is the interaction volume, set at 51 => 1 micron
npts=71
max=npts+mpts
do 5 i=1,npts
  gg(i)=0.
5 continue
do 10 i=npts+1,mpts
  gg(i) = cnf(i-npts-1)
10 continue

sum=0.

do 20 i=1,npts

  prit = -(( real(i)-real(npts/2)-1 )**2/wid**2)
  If(ABS(prit) .LT. 100) then
  f(i) = exp(prit)
  else
  f(i) = 0.0
  end if

  sum=sum+f(i)
  write(3,*) real(i)*h,f(i)
20 continue

snorm=sum

do 40 j=1,mpts+1
  sum=0.
  do 30 i=1,npts
    sum=sum+f(i)*gg(i+j-1)/snorm
30 continue

  psum(j) = sum
* This finds maximum point in numerical output
  If (psum(j) .GT. psum(j-1)) peak = sum
40 continue

* Normalization procedure if desired
do 50 j = 1, mpts+1
  psum(j) = psum(j)/peak
50 continue

close(3)
end

```

```

Function  comprf(npnts,ix,h)
Common cnf(0:1001), x(0:1001)
Common psum(0:1001), ex(0:1001), shift
Real x2(1001),exn(1001),dif(1001)

* unit = 4 is the input file to read the experimental data
Open(unit=4,file='jun20e3p.dat')
Open(unit=5,file='jun203pe.dat')
Open(unit=6,file='jun203pt.dat')

* number to multiply by to match expr points with diff eq
* may need to change this number!!!!!!!!!!!!!!!!!!!!!!!!!!!!!!
  mat = 4

  Do 10 i = 1,npnts
    Read(4,*) x2(i),ex(i)
    Write(5,*) x2(i),ex(i)
10  Continue

* put shift value in k!!!!!!!!!!!!!!!!!!!!!!!!!!!!!!!!!!!!!!
  k=6

  dif(k) = 0.0
  Do 20 i = 0,npnts
    j = mat*i+k
    dif(k) = dif(k) + (ex(i) - psum(j))**2
    write(12,*) psum(j)
20  Continue

  Do 40 i = 0,npnts*mat
    write(6,*)real(i-k-2)*h, psum(i)
40  Continue

  shift = k
  comprf = dif(k)

  close(4)
  close(5)
  close(6)

  Return
  End

```

```

        nlnr2 = (( cn(i+1) - cn(i-1) )**2)*(M-1.0)
        c1 = cnp(i)*nlnr
        c2 = k*( cn(i+1)-cnp(i)+cn(i-1) )
cnf(i) = (c1+c2)/(nlnr+k)-k/4.0*(nlnr2*nlnr)/(nlnr+k)
        cnp(i) = cn(i)
        cn(i) = cnf(i)
80      Continue
        cn(0)=cnp(0)
70      Continue

        Do 76 jj = 0,ix
          Write(1,*)Real(jj)*h,cnf(jj)
76      Continue

*****
* This is the convolution of the Gaussian
  Call filtf(h,ix,wid)

*****
* This is the error fitting routine
  elsq = comprf(npnts,ix,h)

Print*,'error',elsq
Print*,'Dmin',D
Print*,'Width g',Wid
Print*,'shift',shift
Print*,'M',M
300  Format(3x,F7.3,3x,F25.8)

close(1)
close(2)
End

```

APPENDIX A5.1

Analytical explanation of convolution

The convolution of two functions by definition is given by:

$$g(x) * h(x) = \int_{-\infty}^{\infty} g(X) f(x-X) dX$$

The functions of interest are:

$$g(x) = \text{erfc}\left(\frac{x}{2\sqrt{Dt}}\right)$$

and:

$$f(x) = e^{-\frac{x^2}{\sigma^2}}$$

This will produce the following mathematical form:

$$g(x) * f(x) = \int_{-\infty}^{\infty} \text{erfc}\left(\frac{X}{2\sqrt{Dt}}\right) e^{-\frac{(x-X)^2}{\sigma^2}} dX$$

A numerical solution was found for this since this was to be used in a least squares fitting routine. The numerical solution was written in Fortran and is shown in appendix A5.3.

APPENDIX A5.2

Analytical model and fit for interreaction volume

The interaction volume can be estimated by starting with a generic gaussian intensity profile given by:

$$I(x, y) = I_o e^{-\frac{(x^2+y^2)}{\sigma^2}}$$

Integrating with respect to x and y will give the following:

$$I = I_o \int_{-\infty}^{\infty} dx \int_{-\infty}^{y_o} e^{-\frac{x^2+y^2}{\sigma^2}} dy$$

$$I = I_o \sqrt{\pi} \sigma \int_{-\infty}^{y_o} e^{-\frac{y^2}{\sigma^2}} dy$$

This integral has an analytic solution of:

$$I = \frac{\pi}{2} \sigma^2 I_o \left[\operatorname{erf}\left(\frac{y_o}{\sigma}\right) + 1 \right]$$

The slope of this equation can be found by taking the derivative with respect to y_o .

This is useful since a slope can be found from the linescan obtained from the x-ray analysis. The derivative of the above equation is given by:

$$I'(y_o) = \sqrt{\pi} I_o \sigma e^{-\frac{y_o^2}{\sigma^2}}$$

Using $y_o = 0$, this will be the center of the of the linescan and plugging this back into the intensity equation and its derivative gives the following:

$$I(y_o=0) = \frac{\pi}{2} \sigma^2 I_o$$

and

$$I'(y_o=0) = \sqrt{\pi} I_o \sigma$$

Dividing I by I' will give the following:

$$\frac{I}{I'} = \frac{\sqrt{\pi} \sigma}{2}$$

At $y_o = 0$ the intensity, I, will be at one half the maximum intensity, $1/2 I_o$. Taking two pieces of glass with a few differences in the elemental make up and pressing them tightly together then polishing will produce the desired sample for scanning. The x-ray line scan for this is shown in the text. The slope for the two lines came out to be 4.558 for the calcium slope and 4.3578 for the potassium slope. I was esitimated to be 2.42 and 2.52. Sigma was then found to be 0.60 and 0.65 for the two different curves. The FWHM of the guassian shape can by using the following:

$$y_{\frac{1}{2}} = \sigma \sqrt{\ln 2}$$

$$FWHM = 2 \sigma \sqrt{\ln 2}$$

Using this the interaction volume came out to be approximately 0.97 micrometers for one curve and 1.0 micrometers for the other.

VITA[✓]

Kenneth Hial Church

Candidate for the Degree of

Doctor of Philosophy

Disertation: DESIGN AND CHARACTERIZATION OF OPTICAL WAVEGUIDES FOR INTEGRATED LASERS

Major Field: Electrical Engineering

Biographical:

Personal Data: Born in Casper, Wyoming, on December 13, 1962, the son of Hial and Bobbie Church.

Education: Graduated from Kimball County High School, Kimball, Nebraska in May 1981; received an Associates degree from Casper College, Casper, Wyoming in May 1985. Received a Bachelor of Science degree in Physics Engineering and a Bachelor of Science degree in Electrical Engineering from Oklahoma Christian University of Science and Arts in Oklahoma City, Oklahoma in May 1988 and May 1989, respectively. Received a Master of Science degree in Electrical Engineering from Oklahoma State University, Stillwater, Oklahoma in 1991. Completed the requirements for the Doctor of Philosophy degree in Electrical Engineering at Oklahoma State University in December 1994.

Experience: Worked as a lab technician at Oklahoma Christian University; worked at Frontier Engineering during masters program; worked as a research assistant for four years in the Center for Laser Research.

Professional Memberships: IEEE, Toastmasters, OSA